

Multiplying microwave photons by inelastic Cooper-pair tunneling

Juha Leppäkangas,¹ Michael Marthaler,¹ Dibyendu Hazra,^{2,3}
 Salha Jebari,^{2,3} Göran Johansson,⁴ and Max Hofheinz^{2,3}

¹*Institut für Theoretische Festkörperphysik, Karlsruhe Institute of Technology, D-76128 Karlsruhe, Germany*

²*Université Grenoble Alpes, INAC-SPSMS, F-38000 Grenoble, France*

³*CEA, INAC-SPSMS, F-38000 Grenoble, France*

⁴*Microtechnology and Nanoscience, MC2, Chalmers University of Technology, SE-412 96 Göteborg, Sweden*

The interaction between propagating microwave fields and Cooper-pair tunneling across a DC voltage-biased Josephson junction can be highly nonlinear. We show theoretically that this nonlinearity can be used to convert an incoming single microwave photon into an outgoing n -photon Fock state in a different mode. In this process the Coulomb energy released by Cooper-pair tunneling is transferred to the outgoing Fock state, providing energy gain. The conversion can be made reflectionless (impedance-matched) so that all incoming photons are converted to n -photon states. With realistic parameters multiplication ratios $n > 2$ can be reached. By cascading two to three such multiplication stages, the outgoing Fock-states can be sufficiently large to accurately discriminate them from vacuum with linear post-amplification and classical power measurement, implying that our scheme can be used as single-photon detector for itinerant microwave photons without dead time.

PACS numbers: 42.65.-k, 74.50.+r, 85.25.Cp, 85.60.Gz

Introduction: The ability to measure light at the single or few-photon level is a key ingredient of most quantum systems in the optical or the microwave domain. In the optical domain, single-photon detectors (SPD) based on avalanche photo diodes or superconducting nanowires are available and allow to work with very low average photon rates. They are the workhorse of most quantum optics experiments and fundamental research methods, such as quantum state tomography [1]. Together with the creation of nonclassical light they can also be used for quantum communication [2,3] and optical quantum computing [4,5].

In the microwave domain, inspite of important theoretical and experimental developments [6–12] a true SPD of itinerant microwaves has not yet been realized. Instead readout of quantum devices relies on linear parametric amplifiers with noise levels very close to the standard quantum limit of $\frac{1}{2}$ photons. They have allowed for the development of the field of circuit quantum electrodynamics [13–15]. However their use for fields with photon rates less than 1 photon \times bandwidth implies averaging over long times in order to beat the small signal to noise ratio. A true microwave SPD would therefore allow for a host of new possibilities.

We propose building such a device based on inelastic charge tunneling [16–20]. The technological progress in microwave control and detection schemes based on linear amplifiers has allowed not to only address charge transport but also the associated generation of quantum microwaves [21–35]. It has been demonstrated that a Josephson junction, embedded in a superconducting microwave circuit, exhibits a very non-linear light-charge interaction. This is a diverse source of unconventional optoelectronic phenomena, such as production of antibunched photons [36,37], nonclassical photon pairs [21,25,27], multi-photon Fock states [38], and cavity

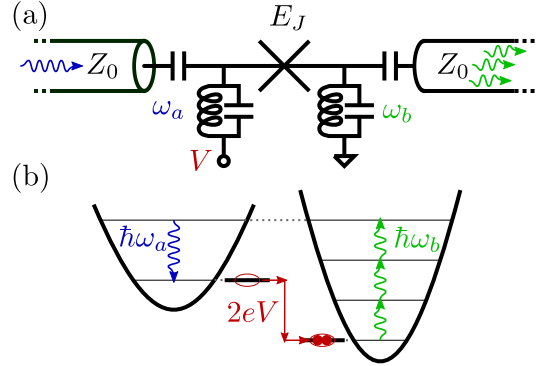


FIG. 1: (a): We investigate microwave radiation in a transmission line connected to two microwave resonators, with resonance frequencies ω_a and ω_b , and a Josephson junction with coupling energy E_J . When impedance matched, an incoming photon of frequency ω_a deterministically converts into n outgoing photons of average frequency ω_b . (b): The energy diagram of photon tripling with slight frequency down-conversion. Energy is absorbed from the Cooper-pair tunneling event, $\hbar\omega_a + 2eV = 3\hbar\omega_b$. Generally, it is possible to up-convert ($\omega_a > \omega_b$) and down-convert ($\omega_a < \omega_b$) incoming microwave photons.

squeezing and multi-stability [39–41], without an external microwave drive.

In this paper, we show theoretically how inelastic Cooper-pair tunneling across a voltage-biased Josephson junction multiplies propagating microwave photons. We consider the microwave circuit depicted in Fig. 1, including two resonators connected by a Josephson junction. Incoming photons from the left-hand side transmission line interact with the Josephson junction, which creates a reflected field to the left and a converted field to the right of the Josephson junction. We find an impedance

matched situation, where a single incoming photon deterministically converts into an outgoing multi-photon Fock state. The Coulomb energy released in the simultaneous Cooper-pair tunneling event, $2eV$, is absorbed by the creation of n photons, $2eV + \hbar\omega_{\text{in}} = n\hbar\omega_{\text{out}}$ and therefore allows for energy gain in this conversion process, i.e. the outgoing photons can have an average frequency close to the incoming one or even higher.

We find that in an experimentally feasible setup several photons can be created from a single-photon input. An efficient photon-number amplification is also possible for a multi-photon input, allowing for cascaded amplification in a setup similar to a photomultiplier tube in the optical domain. We show that it is realistic to create enough photons in two or three multiplication stages for a single microwave photon to be detected with a high fidelity via subsequent linear detection. This scheme of microwave photodetection is qualitatively different from other recent proposals, including single-photon absorption in a phase-qubit type system [6–8], in a lambda-type system [10, 11], or in a driven three-level system [9,12]. Here, the photodetection occurs through direct field amplification and does not include transitions in an artificial atom. The device is then expected to detect photons without any dark time, work with large detection bandwidths and also up to very high microwave frequencies, limited only by the superconducting energy gap.

Model: The semi-infinite transmission lines (TL) are connected to two resonators (see Fig. 1), which impose boundary conditions [2,42]

$$\hat{a}_{\text{in}}(t) + \hat{a}_{\text{out}}(t) = \sqrt{\gamma_a} \hat{a}(t) \quad (1)$$

$$\hat{b}_{\text{in}}(t) + \hat{b}_{\text{out}}(t) = \sqrt{\gamma_b} \hat{b}(t). \quad (2)$$

The photon annihilation (creation) operator $\hat{a}^{(\dagger)}$ corresponds to the standard description of the local field in the left-hand side resonator and $\hat{b}^{(\dagger)}$ in the right-hand side resonator. We have $[\hat{a}, \hat{a}^\dagger] = 1$ and $[\hat{b}, \hat{b}^\dagger] = 1$, other cavity commutators vanish. The operator $\hat{a}_{\text{in}}^{(\dagger)}(t)$ annihilates (creates) an incoming left-hand side TL photon at time t . We have $[\hat{a}_{\text{in}}(t), \hat{a}_{\text{in}}^\dagger(t')] = \delta(t - t')$ and similarly for the out-field operators $\hat{a}_{\text{out}}^{(\dagger)}(t)$ and operators $\hat{b}_{\text{in/out}}^{(\dagger)}(t)$. These are connected to operators of fixed frequencies as $\hat{a}_{\text{in/out}}(\omega) = (1/\sqrt{2\pi}) \int dt e^{i\omega t} \hat{a}_{\text{in/out}}(t)$, which satisfy $[\hat{a}_{\text{in/out}}(\omega), \hat{a}_{\text{in/out}}^\dagger(\omega')] = \delta(\omega - \omega')$ [42,43]. The decay rate $\gamma_{a/b}$ of the cavity field in the corresponding TL defines the bandwidth of the resonator a/b .

The field operators additionally follow the Heisenberg equations of motion [42]

$$\dot{\hat{a}}(t) = \frac{i}{\hbar} [H_0 + H_J, \hat{a}(t)] - \frac{\gamma_a}{2} \hat{a}(t) + \sqrt{\gamma_a} \hat{a}_{\text{in}}(t) \quad (3)$$

$$\dot{\hat{b}}(t) = \frac{i}{\hbar} [H_0 + H_J, \hat{b}(t)] - \frac{\gamma_b}{2} \hat{b}(t) + \sqrt{\gamma_b} \hat{b}_{\text{in}}(t). \quad (4)$$

Here $H_0 = \hbar\omega_a \hat{a}^\dagger \hat{a} + \hbar\omega_b \hat{b}^\dagger \hat{b}$ is the resonator Hamiltonian. The interaction between them is provided by the

Josephson Hamiltonian,

$$H_J = -E_J \cos \left[\omega_J t + g_a (\hat{a} + \hat{a}^\dagger) - g_b (\hat{b} + \hat{b}^\dagger) \right], \quad (5)$$

where the Josephson frequency $\omega_J = 2eV/\hbar$ accounts for the DC voltage bias and the dimensionless coupling $g_{a/b} = \sqrt{\pi Z_{a/b}/R_Q}$ compares the characteristic impedance of the resonator a/b to the resistance quantum $R_Q = h/4e^2$.

Single-photon input: For a single-photon input at frequency $\omega_{\text{in}} \approx \omega_a$, and for voltage bias $\omega_J = n\omega_b - \omega_a$, we can simplify the Josephson Hamiltonian by taking the rotating-wave approximation (the effect of neglected terms is analyzed below in the section "imperfections"),

$$H_J^{\text{RWA}} = \hbar\epsilon_I \hat{a} (\hat{b}^\dagger)^n e^{-i\omega_J t} + \text{H.c.} \quad (6)$$

This creates n photons to oscillator b from a single photon in oscillator a , and vice versa. The amplitude of this process is

$$\epsilon_I = i^{n+1} \frac{1}{n!} \frac{E_J}{2\hbar} g_a g_b^n e^{-g_a^2/2 - g_b^2/2}. \quad (7)$$

Here, we can straightforwardly solve the n -photon scattering element analytically. Using an input-output approach similar to developed in Ref. [44], we obtain [42]

$$\begin{aligned} \langle \hat{b}_{\text{out}}(p_1) \dots \hat{b}_{\text{out}}(p_n) \hat{a}_{\text{in}}^\dagger(\omega_{\text{in}}) \rangle &= \frac{-in! \epsilon_I}{(2\pi)^{(n-1)/2}} \times \quad (8) \\ \frac{\alpha(\omega_{\text{in}})}{1 + |\epsilon_n|^2} \beta(p_1) \dots \beta(p_n) \delta(\omega_{\text{in}} + \omega_J - p_1 - \dots - p_n). \end{aligned}$$

The expectation value is taken with respect to the vacuum and, for simplicity, we assume $\omega_{\text{in}} = \omega_a$ (more general formula is given in the Supplemental Material). The normalized and dimensionless amplitude ϵ_n has the form

$$\epsilon_n = 2\sqrt{(n-1)!} \frac{\epsilon_I}{\sqrt{\gamma_a \gamma_b}}, \quad (9)$$

and the functions $\alpha(\omega) = \sqrt{\gamma_a}/(i\omega_a - i\omega + \gamma_a/2)$, $\beta(\omega) = \sqrt{\gamma_b}/(i\omega_b - i\omega + \gamma_b/2)$, describe the effect of the resonator bandwidths. We find that the created n -photon state is entangled in frequency: it is the superposition of all possible out-field frequency combinations that sum up to $\omega_a + \omega_J$. This type of correlations are nonclassical and, for example, can violate a Bell inequality for the position and time [45]. By Fourier transforming one obtains the shape of the multi-photon Fock state in the time domain [43]. In case of a two-photon state one gets $\int dp_1 \int dp_2 e^{i(p_1 t_1 + p_2 t_2)} \beta(p_1) \beta(p_2) \delta(\omega_{\text{in}} + \omega_J - p_1 - p_2) \propto e^{-\gamma_b |t_1 - t_2|/2}$. For a narrow input frequency but wide $\beta(p)$ the output is highly bunched.

The average number of outwards propagating photons on side b can be solved analytically by using the scattering matrix or by a direct linearization of the problem [42].

We get (assuming $\omega_{\text{in}} = \omega_a$)

$$\begin{aligned} N_{\text{out}} &= \int d\omega \int d\omega' \langle \hat{a}_{\text{in}}(\omega_{\text{in}}) \hat{b}_{\text{out}}^\dagger(\omega') \hat{b}_{\text{out}}(\omega) \hat{a}_{\text{in}}^\dagger(\omega_{\text{in}}) \rangle \\ &= n \frac{4|\epsilon_n|^2}{(1 + |\epsilon_n|^2)^2} \end{aligned} \quad (10)$$

One sees that when $|\epsilon_n| \rightarrow 0$ or $|\epsilon_n| \rightarrow \infty$, the incoming field is totally reflected ($N_{\text{out}} = 0$). When $|\epsilon_n| = 1$, the incoming photon is perfectly converted ($N_{\text{out}} = n$). This reflectionless multiplication corresponds to

$$E_J = \hbar \sqrt{\gamma_a \gamma_b} \frac{n!}{\sqrt{(n-1)!}} \frac{e^{g_a^2/2 + g_b^2/2}}{g_a g_b^n}. \quad (11)$$

This central result states that, irrespective of the resonator quality factors, one can always achieve a perfect photon multiplication if E_J is chosen correctly. This is an important result for an experimental realization, since when the Josephson junction is realized in a SQUID geometry, the Josephson coupling can be tuned externally to the optimal value via an applied magnetic field.

Multi-photon input: We now assess whether several multiplication stages can be cascaded. For this we determine how the multiplier handles input signals with higher photon numbers, generated by preceding stages.

For a multi-photon input the Hamiltonian under the rotating-wave approximation is generalized to [42,46]

$$\begin{aligned} H_J^{\text{RWA}} &= (i)^{n+1} \frac{E_J}{2} \sum_{k=0}^{\infty} A_{k+n,k}(g_b) |k+n\rangle_b \langle k|_b \\ &\times \sum_{l=0}^{\infty} A_{l+1,l}(g_a) |l\rangle_a \langle l+1|_a + \text{H.c.}, \end{aligned} \quad (12)$$

where

$$A_{k+n,k}(g) = g^n e^{-g^2/2} \sqrt{\frac{k!}{(k+n)!}} L_k^{(n)}(g^2), \quad (13)$$

and $L_k^{(n)}(x)$ is the generalized Laguerre polynomial. The Hamiltonian of Eq. (6) is obtained within the approximation $L_k^{(n)} \approx (k+n)!/k!n!$, which is exact if $k=0$ (single-photon input), whereas for $\sqrt{k}g \gtrsim 1$ corrections are essential [38,39,41].

To simplify the problem, we approximate the secondary input by an appropriate coherent-state pulse. This allows for a master-equation type model for the dynamics of the resonator fields [42]. To qualitatively describe the bunching of converted photons in the time domain (see "single-photon input"), we choose a coherent-state pulse with the waveform

$$\epsilon(t) = \sqrt{\frac{N_{\text{in}} \gamma_{1st}}{2}} \exp \left[-i\omega_a t - \frac{\gamma_{1st}|t-t_0|}{2} \right]. \quad (14)$$

The pulse has on average $\int dt |\epsilon(t)|^2 = N_{\text{in}}$ photons and

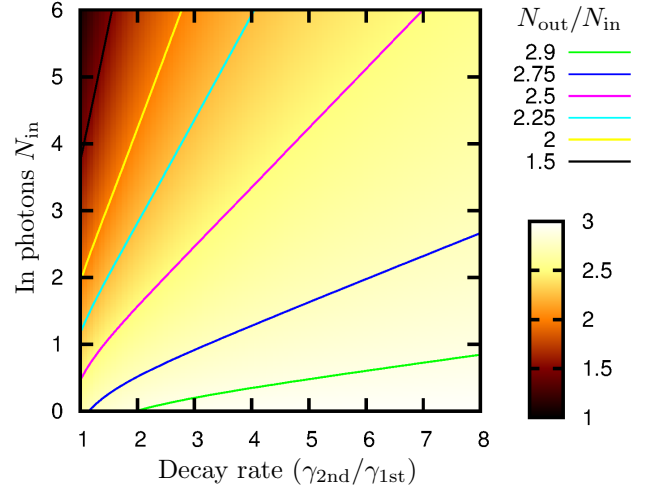


FIG. 2: Numerically evaluated multiplication efficiency $N_{\text{out}}/N_{\text{in}}$ as a function of cavity decay rate γ_{2nd} and average input photon number N_{in} when biased at the photon-tripling resonance ($n=3$). We consider an incoming coherent pulse of width γ_{1st} with waveform of Eq. (14). The perfect conversion occurs in the limit $\gamma_{2nd}/\gamma_{1st} \rightarrow \infty$, where $N_{\text{out}}/N_{\text{in}} \rightarrow n$.

at time t_0 the peak of the wavepacket reaches the resonator a . The width is defined by the primary-input cavity b decay, $\gamma_{1st} \equiv \gamma_b$.

In Fig. 2, we plot the photon-number multiplication $N_{\text{out}}/N_{\text{in}}$ as a function of identical (second-state) resonator bandwidths γ_{2nd} and the incoming photon number N_{in} , in the case $n=3$, $\epsilon_n=1$ (reflectionless single-photon multiplication), and $g_a=g_b=1$. The output photon number approaches $N_{\text{out}}/N_{\text{in}}=n$ when $\gamma_{2nd}/\gamma_{1st} \rightarrow \infty$. We observe that increasing N_{in} decreases the multiplication efficiency $N_{\text{out}}/N_{\text{in}}$. In a linear system ($n=1$) this is a constant for fixed $\gamma_{2nd}/\gamma_{1st}$. This reflects the fact that in the non-linear case the impedance matching depends on the photon numbers of the oscillators. Increase in the decay rate γ_{2nd} increases amplification efficiency, since faster decay keeps the average cavity photon numbers closer to zero. We find practically a linear dependence between the number of incoming photons N_{in} and secondary bandwidth $\gamma_{2nd}/\gamma_{1st}$, when the multiplication efficiency is kept constant (solid contour lines). In additional simulations we find that tuning ϵ_l to higher values can increase the multiplication efficiency of high photon number pulses [42]. We expect that this increase is even more pronounced for Fock states actually produced by previous stages. The multiplication efficiency can also be increased by decreasing the impedance of the input resonator (g_a) [42], the tradeoff being higher rate for emission without input (see "imperfections"). The estimate shown in Fig. 2 is therefore rather cautious.

We also find that the width of the outgoing pulse is approximately defined by γ_{1st} . We conclude that a cascaded photon multiplication is most efficient when the bandwidth of subsequent amplification stages is gradually increased.

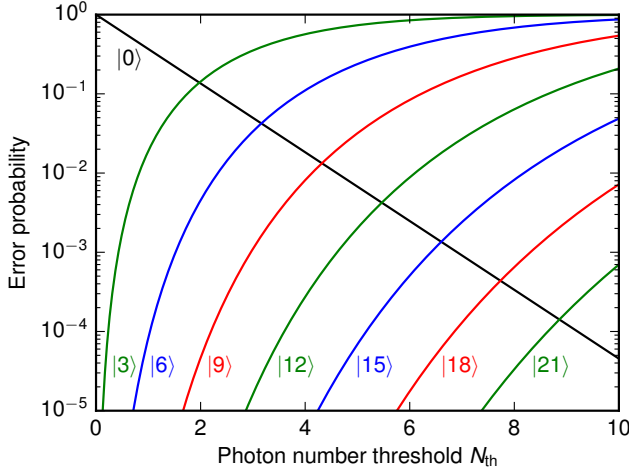


FIG. 3: Error probabilities for photon detection using a linear quantum-limited phase-preserving amplifier at the output of a $\times n$ photomultiplier. The error rates are plotted as a function of threshold N_{th} of photons per bandwidth. The black line labeled $|0\rangle$ indicates the dark-count probability (false click) within an inverse bandwidth. The lines labeled $|n\rangle$ with $n > 0$ show the probability of a $|n\rangle$ state not triggering a click.

Single-photon detection: This photomultiplier can be transformed into a single-photon detector by placing a quantum-limited (phase-preserving) amplifier at the output of the photomultiplier and measuring the instantaneous output power within the output bandwidth of the photomultiplier. In Fig. 3, we plot the resulting dark-count probability and the probability of missed photons as a function of chosen threshold N_{th} of photons per bandwidth and multiplication factor n [42]. We find that already for a multiplication ratio of $n = 3 \times 3 = 9$ we can obtain a quantum efficiency of approximately 0.9 for a dark count rate of $10^{-3} \times \text{bandwidth}$. Much lower dark-count rates for this photon number can be obtained if lower quantum efficiencies are sufficient. Unlike existing designs [7,11], such an amplifier can detect another photon immediately after a previous detection event. We also expect it to be able to resolve photon numbers, even though the efficiency will decrease with photon number.

Imperfections: The main degrading effects for single-photon detection are (i) reflection induced by junction voltage fluctuations and (ii) emission in the absence of input (due to processes neglected in the rotating-wave approximation). The former effect can be estimated via quasistatic voltage fluctuations and the latter using a perturbative approach developed in Refs. [21,25,26].

The charge transport as well as finite temperature induce low-frequency voltage fluctuations in the biasing circuitry. For a low-Ohmic TL the effect temperature is usually dominating [26]. For a 50Ω TL at 20 mK the fluctuations broaden the emission spectrum by $\gamma_{\text{th}}/2\pi \approx k_B T Z_0 / \hbar R_Q \approx 20 \text{ MHz}$.

The average induced single-photon reflection probabil-

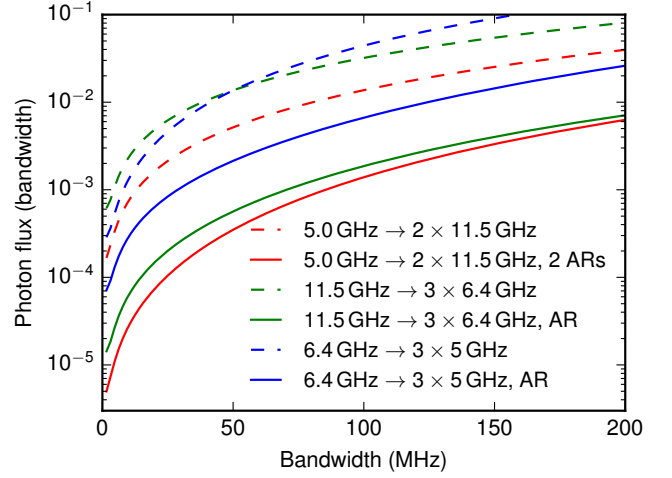


FIG. 4: Spontaneous emission at different stages of a cascaded photomultiplier discussed in the text. We plot the total photon flux (in units of γ) at out-frequency ω_b within bandwidth 1 GHz as a function of resonator bandwidths $\gamma/2\pi$ with (solid lines) and without (dashed lines) an anti-resonance (AR) in the impedance seen by the junction. We consider the case $g_{a/b} = 1$ and a thermal broadening $\gamma_{\text{th}}/2\pi = 20 \text{ MHz}$. For more details see [42].

ity (when $|\epsilon_n| = 1$, $\omega_{\text{in}} = \omega_a$, and $\gamma_a = \gamma_b \equiv \gamma$) is estimated to be $\gamma_{\text{th}}/(n\gamma + \gamma_{\text{th}})$ [42]. Therefore, to minimize the reflection due to low-frequency noise in the voltage, the resonator bandwidths should satisfy $n\gamma \gg \gamma_{\text{th}}$. The reflection decreases with increasing n due to widening of the effective multi-photon resonance condition.

When biased $2eV < \hbar\omega_b$, such as in the case of photon doubling with frequency down-conversion, radiation at the out resonance frequency ω_b without input photons can only arise from upward thermal fluctuations of the junction voltage. An example is creating $2 \times 5 \text{ GHz}$ photons from a single 7 GHz photon, where we find that even resonator bandwidths up to 500 MHz result in weak spurious emission rates ($< 10^{-3}\gamma$ with $\gamma_{\text{th}}/2\pi = 20 \text{ MHz}$).

When biased $2eV/\hbar = \omega_J > \hbar\omega_b$, no thermal energy is needed to create radiation to ω_b , since zero-point fluctuations allow for spontaneous emission of one photon to oscillator b and another photon to mode at $\delta\omega = \omega_J - \omega_b > 0$ of the relevant electromagnetic environment. We find that the rate of this process is approximately $\propto 1/[g_a^2 g_b^{2(n-1)}]$ [42]. Therefore, by increasing dimensionless coupling $g_{a/b}$, we decrease spontaneous emission. However, values much higher than $g \sim 1$ are experimentally challenging and therefore our analysis concentrates on the feasible case $g_{a/b} = 1$. The rates of these spontaneous emission events are also proportional to the real parts of the impedance at ω_b and $\delta\omega$, and can therefore be reduced by engineering an anti-resonance in the impedance at $\delta\omega$, as demonstrated below.

In Fig. 4, we plot the photon flux due to spontaneous emission in units of γ in several situations with

$2eV/\hbar > \hbar\omega_b$. One scheme for cascaded photon multiplication is to perform two or three consecutive photon triplings, each with slight frequency down-conversion. An estimate for flux of spontaneous emission in each multiplication step is the process $6.4 \text{ GHz} \rightarrow 3 \times 5 \text{ GHz}$. We find that with single anti-resonance, the probability for spurious emission per bandwidth can be kept below 10^{-3} (10^{-2}) when $\gamma/2\pi = 25 \text{ MHz}$ (120 MHz). An alternative cascasion scheme is to start with up-converting photon doubling and continue with two down-converting photon triplings. (Numerical analysis shows that photon tripling with up-conversion is rather noisy and should be avoided.) In the considered case of strong up-conversion ($5 \text{ GHz} \rightarrow 2 \times 11.5 \text{ GHz}$), the setup produces single photons spontaneously with probability $< 10^{-3}$ per inverse bandwidth up to $\gamma/2\pi = 80 \text{ MHz}$ (obtained using two anti-resonances). The following photon tripling can be made with stronger down-conversion (here $11.5 \text{ GHz} \rightarrow 3 \times 6.4 \text{ GHz}$) and thereby with lower noise. The cycle ends with another photon tripling ($6.4 \text{ GHz} \rightarrow 3 \times 5 \text{ GHz}$). According to results presented in section "multi-photon input", the two latter multiplications should be done with an increased bandwidth, such as $\gamma/2\pi = 150 \text{ MHz}$ for initial multiplication with $\gamma/2\pi = 50 \text{ MHz}$. The most undesirable spontaneous emission is at the first amplification stage since it is followed by other amplifications. Spontaneous emission at subsequent stages likely stays below the threshold of the power detection. Keeping the first rate below the dark-count rate originating in the power detection, we achieve a situation where the dark-count rate is not limited by spontaneous emission.

Summary: We have shown that inelastic Cooper-pair tunneling can convert propagating single microwave pho-

tons to multi-photon Fock states. In comparison to photon-number doubling in parametric down conversion [2], the important difference, here, is that the energy absorbed from charge transport provides energy gain to the conversion process. The resulting Fock states are frequency and time-bin entangled, an outcome which could be very relevant for quantum-information applications.

Further, we have shown that it is possible to detect single propagating microwave photon through cascaded multiplication, followed by linear amplification and instantaneous power detection. This scheme for microwave photodetection allows detecting another photon immediately after the previous detection event. As the cut-off frequency in our scheme is limited, in principle, only by the superconducting energy gap, we expect that the photon multiplication can be realizable in a very broadband frequency range, extending from a few GHz up to a few 100 GHz, depending on the material used. Using a similar device backwards provides an engineered bath where multi-photon absorption is dominant. This is useful, for example, for 'cat codes' [47] which encode a error-protected logical qubit in superpositions of coherent states.

JL and MM acknowledge financial support from DFG Grant No. MA 6334/3-1. DH, SJ, and MH acknowledge financial support from Grenoble Nanosciences Foundation and from the European Research Council under the European Union's Seventh Framework Programme (FP7/2007-2013) / ERC Grant agreement No 278203 – WiQOJo. GJ acknowledges financial support from the Swedish Research Council and the Knut and Alice Wallenberg Foundation.

-
- ¹ A. I. Lvovsky and M. G. Raymer, Rev. Mod. Phys. **81**, 299 (2009).
 - ² D. F. Walls and G.J. Milburn, *Quantum Optics* (Springer, Berlin, 2008).
 - ³ N. Gisin, G. Ribordy, W. Tittel, and H. Zbinden, Rev. Mod. Phys. **74**, 145 (2002).
 - ⁴ N. C. Menicucci, P. van Loock, M. Gu, C. Weedbrook, T. C. Ralph, and M. A. Nielsen, Phys. Rev. Lett. **97**, 110501 (2006).
 - ⁵ P. Kok, W. J. Munro, K. Nemoto, T. C. Ralph, J. P. Dowling, and G. J. Milburn, Rev. Mod. Phys. **79**, 135 (2007).
 - ⁶ G. Romero, J. J. Garcia-Ripoll, and E. Solano, Phys. Rev. Lett. **102**, 173602 (2009).
 - ⁷ Y.-F. Chen, H. S. Sendelbach, L. Maurer, S. T. Merkel, E. J. Pritchett, F. K. Wilhelm, and R. McDermott, Phys. Rev. Lett. **107**, 217401 (2011).
 - ⁸ L. C. G. Govia, E. J. Pritchett, S. T. Merkel, D. Pineau, and F. Wilhelm, Phys. Rev. A **86**, 032311 (2012).
 - ⁹ S. R. Sathyamoorthy, L. Tornberg, A. F. Kockum, B. Q. Baragiola, J. Combes, C. M. Wilson, T. M. Stace, and G. Johansson, Phys. Rev. Lett. **112**, 093601 (2014).
 - ¹⁰ K. Koshino, K. Inomata, Z. Lin, Y. Nakamura, and T. Yamamoto, Phys. Rev. A **91**, 043805 (2015).
 - ¹¹ K. Inomata, Z. Lin, K. Koshino, W. D. Oliver, J.-S. Tsai, T. Yamamoto, Y. Nakamura, Nature Comm. **7**, 12303 (2016).
 - ¹² O. Kyriienko and A. S. Sorensen, Phys. Rev. Lett. **117**, 140503 (2016).
 - ¹³ J. Clarke and F. K. Wilhelm, Nature (London) **453**, 1031 (2008).
 - ¹⁴ R. J. Schoelkopf and S. M. Girvin, Nature (London) **451**, 664 (2008).
 - ¹⁵ M. H. Devoret and R. J. Schoelkopf, Science **339**, 1169 (2013).
 - ¹⁶ G.-L. Ingold and Yu. V. Nazarov, in *Single Charge Tunneling: Coulomb Blockade Phenomena in Nanostructures*, edited by H. Grabert and M. H. Devoret (Plenum, New York, 1992), p.21.
 - ¹⁷ M. H. Devoret, D. Esteve, H. Grabert, G.-L. Ingold, H. Pothier, and C. Urbina, Phys. Rev. Lett. **64**, 1824 (1990).
 - ¹⁸ S. M. Girvin, L. I. Glazman, M. Jonson, D. R. Penn, and M. D. Stiles, Phys. Rev. Lett. **64**, 3183 (1990).
 - ¹⁹ T. Holst, D. Esteve, C. Urbina, and M. H. Devoret, Phys. Rev. Lett. **73**, 3455 (1994).
 - ²⁰ J. Leppäkangas, E. Thuneberg, R. Lindell, and P. Hak-

- nen, Phys. Rev. B **74** 054504 (2006).
- ²¹ M. Hofheinz, F. Portier, Q. Baudouin, P. Joyez, D. Vion, P. Bertet, P. Roche, and D. Esteve, Phys. Rev. Lett. **106**, 217005 (2011).
- ²² J.-C. Forgues, C. Lupien, and B. Reulet, Phys. Rev. Lett. **114**, 130403 (2015).
- ²³ O.-P. Saira, M. Zgirski, K. L. Viitanen, D. S. Golubev, J. P. Pekola, Phys. Rev. Applied **6**, 024005 (2016).
- ²⁴ C. W. J. Beenakker and H. Schomerus, Phys. Rev. Lett. **93** 096801 (2004).
- ²⁵ J. Leppäkangas, G. Johansson, M. Marthaler, and M. Fogelström, Phys. Rev. Lett. **110**, 267004 (2013).
- ²⁶ J. Leppäkangas, G. Johansson, M. Marthaler, and M. Fogelström, New J. Phys. **16**, 015015 (2014).
- ²⁷ M. Trif and P. Simon, Phys. Rev. B **92**, 014503 (2015).
- ²⁸ O. Parlavécchio, C. Altimiras, J.-R. Souquet, P. Simon, I. Safi, P. Joyez, D. Vion, P. Roche, D. Esteve, and F. Portier, Phys. Rev. Lett. **114** 126801 (2015).
- ²⁹ F. Qassemi, A. L. Grimsom, B. Reulet, and A. Blais, Phys. Rev. Lett. **116** 043602 (2009).
- ³⁰ F. Hassler and D. Otten, Phys. Rev. B **92**, 195417 (2015).
- ³¹ A. Cottet, T. Kontos, and B. Doucot, Phys. Rev. B **91**, 205417 (2015).
- ³² J. Jin, M. Marthaler and G. Schön, Phys. Rev. B **91**, 085421 (2015).
- ³³ J. Jin, M. Marthaler, P. Q. Jin, D. Golubev and G. Schön New J. Phys. **15**, 025044 (2013).
- ³⁴ J.-R. Souquet, M.J. Woolley, J. Gabelli, P. Simon, A. A. Clerk, Nature Communications **5**, 5562 (2014).
- ³⁵ J. Leppäkangas, M. Fogelström, M. Marthaler, and G. Johansson, Phys. Rev. B **93** 014506 (2016).
- ³⁶ J. Leppäkangas, M. Fogelström, A. Grimm, M. Hofheinz, M. Marthaler, and G. Johansson, Phys. Rev. Lett. **115** 027004 (2015).
- ³⁷ S. Dambach, B. Kubala, V. Gramich, and J. Ankerhold, Phys. Rev. B **92**, 054508 (2015).
- ³⁸ J.-R. Souquet and A. A. Clerk, Phys. Rev. A **93**, 060301(R) (2016).
- ³⁹ M. Marthaler, J. Leppäkangas, and J. H. Cole, Phys. Rev. B **83**, 180505(R) (2011).
- ⁴⁰ A. D. Armour, M. P. Blencowe, E. Bahimi, A. J. Rimberg, Phys. Rev. Lett. **111** 247001 (2013).
- ⁴¹ V. Gramich, B. Kubala, S. Rocher, J. Ankerhold, Phys. Rev. Lett. **111** 247002 (2013).
- ⁴² See the Supplemental Material for details.
- ⁴³ R. Loudon, *The Quantum Theory of Light* (Oxford University, New York, 2010).
- ⁴⁴ S. Fan S, S. E. Kocabas, and J.-T. Shen, Phys. Rev. B **82** 063821 (2010).
- ⁴⁵ J. D. Franson, Phys. Rev. Lett. **62**, 2205 (1989).
- ⁴⁶ A. Wünsche, Quantum Opt. **3**, 359 (1991).
- ⁴⁷ N. Ofek, A. Petrenko, R. Heeres, P. Reinhold, Z. Leghtas, B. Vlastakis, Y. Liu, L. Frunzio, S. M. Girvin, L. Jiang, M. Mirrahimi, M. H. Devoret, and R. J. Schoelkopf, Nature **536**, 441 (2016).
- ⁴⁸ B. Peropadre, J. Lindkvist, I.-C. Hoi, C. M. Wilson, J. J. Carcia-Ripoll, P. Delsing, and G. Johansson, New J. Phys. **15**, 035009 (2013).
- ⁴⁹ M. S. Kim, Phys. Rev. A **56**, 3175 (1997).
- ⁵⁰ C. Altimiras, O. Parlavécchio, P. Joyez, D. Vion, P. Roche, and F. Portier, Appl. Phys. Lett. **103**, 212603 (2013).

Supplemental Material

The supplemental material is organized as follows. In Section I, we derive the Heisenberg equations of motion used in the main part of the article. In Section II, we derive analytical expressions for the single-to-multiphoton scattering matrix and, by properly linearizing the problem, for the conversion probability. In Section III, we derive the Hamiltonian used in the case of a multi-photon input and establish the master-equation approach applicable for the specific case of a coherent-state input. Also additional numerical results on photon multiplication properties are shown. In Section IV, we discuss how multi-photon Fock states can be detected using linear measurement. In Section V, we estimate the effect of finite temperature to conversion probability and photon emission rate in the absence of input radiation.

I. HEISENBERG EQUATIONS OF MOTION

Here, we derive the Heisenberg equations of motion used in the main part of the paper starting from a continuous-mode treatment of the circuit shown in Fig. S1. A similar derivation is given also in many other works, e.g., in Ref. [48]. We consider explicitly the microwave circuit shown in Fig. S1, but this is not the only possible realization of our system. For example, the electromagnetic environment could also consists of two $\lambda/4$ -type resonators, connected by the Josephson junction.

A. Lagrangian and Hamiltonian

The total Lagrangian of the system can be decomposed as

$$\mathcal{L} = \mathcal{L}_L + \mathcal{L}_J + \mathcal{L}_R \quad (\text{S1})$$

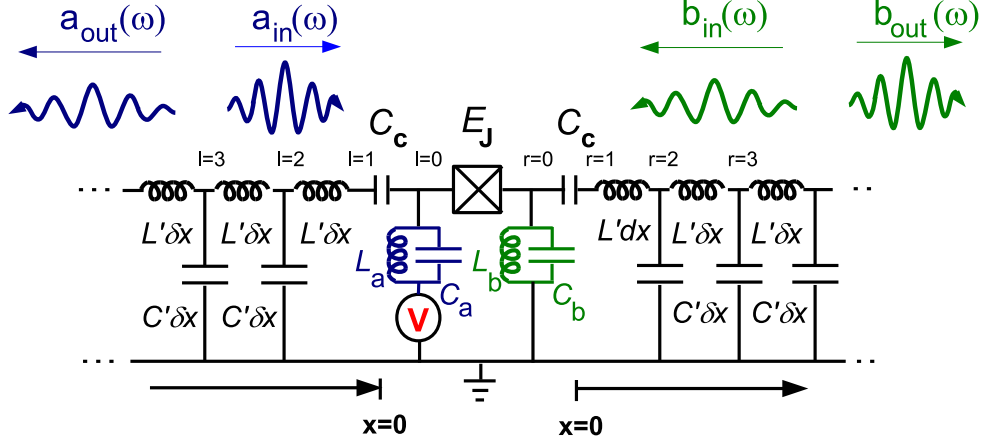


FIG. S1: Lumped-element model of the considered microwave circuit.

The left-hand side Lagrangian splits into $\mathcal{L}_L = \mathcal{L}_{TL} + \mathcal{L}_a$, where the transmission-line part reads

$$\mathcal{L}_{TL} = \sum_{l \geq 2}^{\infty} \frac{\delta x C' (\dot{\Phi}_l + V)^2}{2} - \sum_{l \geq 2}^{\infty} \frac{(\Phi_l - \Phi_{l-1})^2}{2L'\delta x} + \frac{C_c (\dot{\Phi}_1 - \dot{\Phi}_a)^2}{2}. \quad (\text{S2})$$

Here $\Phi_l(t)$ is the magnetic flux of node l and $\dot{\Phi}_l + V$ is the corresponding voltage. This amounts to defining the magnetic flux (time integrated voltage) of the left-hand side transmission line with respect to $\Phi_V = Vt$. The left-hand side oscillator part is

$$\mathcal{L}_a = \frac{C_a \dot{\Phi}_a^2}{2} - \frac{\Phi_a^2}{2L_a}. \quad (\text{S3})$$

Similarly for the oscillator b and the right-hand side transmission line (with the value $V = 0$). The Josephson junction is described by the potential-energy term,

$$\mathcal{L}_J = E_J \cos \left(2\pi \frac{\Phi_V + \Phi_a - \Phi_b}{\Phi_0} \right). \quad (\text{S4})$$

Here E_J is the Josephson coupling energy and $\Phi_0 = h/2e$ is the flux quantum.

The above Lagrangian leads to the left-hand side Hamiltonian

$$H_L \equiv \sum_{i \in L} \dot{\Phi}_i Q_i - \mathcal{L}_L = \sum_{l=2}^M \frac{(Q_l - \delta x C' V)^2}{2\delta x C'} + \sum_{l \geq 2}^N \frac{(\Phi_l - \Phi_{l-1})^2}{2L'\delta x} + \frac{Q_a^2}{2C_a} + \frac{\Phi_a^2}{2L_a} + \frac{Q_a Q_1}{C_a} + \frac{Q_1^2}{2C_s}, \quad (\text{S5})$$

where $Q_i = \partial \mathcal{L} / \partial \dot{\Phi}_i$ and $1/C_s = 1/C_c + 1/C_a$.

For convenience, we can do a shift in the momentum variable and neglect the terms $\propto \delta x C' V$. This does not change the Hamiltonian equations

$$\frac{dQ_i}{dt} = -\frac{\partial H}{\partial \dot{\Phi}_i} \quad (\text{S6})$$

$$\frac{d\dot{\Phi}_i}{dt} = +\frac{\partial H}{\partial Q_i}, \quad (\text{S7})$$

provided that V is a constant. Standard quantization means $\Phi_i \rightarrow \hat{\Phi}_i$ and $Q_i \rightarrow \hat{Q}_i$ with $[\hat{\Phi}_i, \hat{Q}_i] = i\hbar$. Defining the normalized phase, $\hat{\phi}_i \equiv 2\pi \Phi_i / \Phi_0$, we have equivalently $[\hat{\phi}_i, \hat{Q}_i] = i2e$.

B. Transmission line solution

The Heisenberg equations of motion in the transmission line are ($l \geq 2$)

$$\dot{\hat{\Phi}}_i(t) = \frac{i}{\hbar} [\hat{H}, \hat{\Phi}_i] \quad (\text{S8})$$

$$\dot{\hat{Q}}_i(t) = \frac{i}{\hbar} [\hat{H}, \hat{Q}_i]. \quad (\text{S9})$$

These give us

$$\dot{\hat{\Phi}}_l(t) = \frac{\hat{Q}_l}{\delta x C'} \quad (\text{S10})$$

$$\dot{\hat{Q}}_l(t) = \frac{\hat{\Phi}_{l-1} + \hat{\Phi}_{l+1} - 2\hat{\Phi}_l}{\delta x L'}. \quad (\text{S11})$$

In the continuum limit $\delta x \rightarrow 0$, the two equation lead to the Klein-Gordon equation,

$$\hat{\Phi}(x, t) = \frac{1}{L'_i C'_i} \frac{\partial^2 \hat{\Phi}(x, t)}{\partial^2 x}. \quad (\text{S12})$$

We can then establish a solution in the free space ($x < 0$)

$$\hat{\Phi}(x, t) = \sqrt{\frac{\hbar Z_0}{4\pi}} \int_0^\infty \frac{d\omega}{\sqrt{\omega}} \left[\hat{a}_{\text{in}}(\omega) e^{i(k_\omega x - \omega t)} + \hat{a}_{\text{out}}(\omega) e^{i(-k_\omega x - \omega t)} + \text{H.c.} \right], \quad (\text{S13})$$

where $Z_0 = \sqrt{L'/C'}$ and $k_\omega = \omega \sqrt{L'C'}$. Here, the operator $\hat{a}_{\text{in(out)}}^\dagger(\omega)$ creates and the operator $\hat{a}_{\text{in(out)}}(\omega)$ annihilates an incoming (outgoing) propagating photon of frequency ω . We have the commutation relations

$$[\hat{a}_{\text{in}}(\omega), \hat{a}_{\text{in}}^\dagger(\omega')] = \delta(\omega - \omega'), \quad (\text{S14})$$

and similarly for the out-operators. The same derivation also applies for the propagating fields on the right-hand side transmission line.

Narrow bandwidth approximation

If only frequencies close to the resonance frequency ω_a are relevant, we can replace the factor $1/\sqrt{\omega}$ in Eq. (S13) by $1/\sqrt{\omega_a}$. We have then

$$\hat{\Phi}(x, t) = \sqrt{\frac{\hbar Z_0}{4\pi\omega_a}} \int_{-\infty}^\infty d\omega \left[\hat{a}_{\text{in}}(\omega) e^{i(k_\omega x - \omega t)} + \hat{a}_{\text{out}}(\omega) e^{i(-k_\omega x - \omega t)} + \text{H.c.} \right]. \quad (\text{S15})$$

Here, we have also formally extended the integration over frequencies to $-\infty$, even though negative frequencies are not actually defined here. This mathematical redefinition does not change results, when frequencies well below ω_a have negligible contribution, but makes the use of Fourier transformations formally more clear. Within this we write

$$\hat{\Phi}(x, t) = \sqrt{\frac{\hbar Z_0}{2\omega_a}} [\hat{a}_{\text{in}}(t - x/c) + \hat{a}_{\text{out}}(t + x/c) + \text{H.c.}], \quad (\text{S16})$$

where $\hat{a}_{\text{in/out}}(t) = (1/\sqrt{2\pi}) \int_{-\infty}^\infty d\omega e^{-i\omega t} \hat{a}_{\text{in/out}}(\omega)$ and $c = 1/\sqrt{L'/C'}$. We have then commutation relations $[\hat{a}_{\text{in}}(t), \hat{a}_{\text{in}}^\dagger(t')] = \delta(t - t')$. The inverse transformation has the form $\hat{a}_{\text{in}}(\omega) = (1/\sqrt{2\pi}) \int_{-\infty}^\infty dt e^{i\omega t} \hat{a}_{\text{in}}(t)$. Similarly for the out-field operators.

C. Resonator equations

We introduce now the resonator creation and annihilation operators,

$$\hat{\Phi}_a = f \sqrt{\frac{\hbar}{2}} (\hat{a} + \hat{a}^\dagger) \quad (\text{S17})$$

$$\hat{Q}_a = \frac{i}{f} \sqrt{\frac{\hbar}{2}} (\hat{a}^\dagger - \hat{a}). \quad (\text{S18})$$

Here for a free resonator the choice $f^2 = Z_{LC} = \sqrt{L_a/C_a}$ diagonalizes the resonator Hamiltonian, and in this case

$$\hat{\phi} = \frac{2\pi}{\Phi_0} \hat{\Phi}_a = \sqrt{\pi \frac{Z_{LC}}{R_Q}} (\hat{a} + \hat{a}^\dagger). \quad (\text{S19})$$

$\hat{\phi} = (2\pi/\Phi_0) \hat{\Phi}_a = \sqrt{\pi Z_{LC}/R_Q} (\hat{a} + \hat{a}^\dagger)$. The resonance frequency has then the form $\omega_a = \sqrt{1/L_a C_a}$. However, at this point we do not fix Z_{LC} to this value, since the resonator capacitance will be normalized by the coupling capacitance C_c , as derived below. The form of Eq. (S19), however, stays the same, calculated with the renormalized capacitance.

At the resonator boundary ($l = 1$) the Heisenberg equations of motion give

$$\dot{\hat{\Phi}}_1(t) = \frac{\hat{Q}_a}{C_a} + \frac{\hat{Q}_1}{C_s} \quad (\text{S20})$$

$$\dot{\hat{Q}}_1(t) = \frac{\hat{\Phi}_2 - \hat{\Phi}_1}{\delta x L'} \rightarrow -\frac{1}{L'} \frac{\partial \hat{\Phi}(x=0, t)}{\partial x}. \quad (\text{S21})$$

The derivative with respect to x corresponds to the continuum limit $\delta x \rightarrow 0$. A solution for the latter equation is

$$\hat{Q}_1(t) = \sqrt{\frac{\hbar}{4\pi Z_0}} \int_0^\infty \frac{d\omega}{\sqrt{\omega}} [\hat{a}_{\text{in}} e^{-i\omega t} - \hat{a}_{\text{out}} e^{-i\omega t}] + \text{H.c.} = \sqrt{\frac{\hbar}{2\omega_a Z_0}} [\hat{a}_{\text{in}}(t) - \hat{a}_{\text{out}}(t)] + \text{H.c.} \quad (\text{S22})$$

To proceed we now make an important observation. In Eq. (S20), the operator \hat{Q}_1/C_s is characterized by relative size $\omega_c \equiv 1/C_s Z_0$, whereas the time derivative of the phase $\dot{\hat{\Phi}}_1(t)$ by size ω_a . Here, it is always the former term that will dominate (high cut-off frequency), and we can neglect the time derivative of the phase operator. In this limit we get

$$\hat{a}_{\text{out}}(t) - \hat{a}_{\text{in}}(t) = \alpha \hat{a}(t) \quad (\text{S23})$$

$$\alpha = -i \frac{C_s}{C_a} \sqrt{\frac{Z_0}{Z_{LC}}} \sqrt{\omega_a}. \quad (\text{S24})$$

To derive this we have used

$$\hat{Q}_a = i \sqrt{\frac{\hbar}{2Z_{LC}}} [\hat{a}^\dagger(t) - \hat{a}(t)]. \quad (\text{S25})$$

At the junction, the effective Hamiltonian to be used in the Heisenberg equations of motion has the form

$$\begin{aligned} & \hbar \left[\frac{Z_{LC}}{4L_a} (\hat{a} + \hat{a}^\dagger)^2 - \frac{1}{4Z_{LC}C_a} (\hat{a} - \hat{a}^\dagger)^2 \right] + \hat{H}_J + i \frac{1}{C_a} \hat{Q}_1 \sqrt{\frac{\hbar}{2Z_{LC}}} [\hat{a}^\dagger - \hat{a}] = \\ & = \hbar \left[\frac{Z_{LC}}{4L_a} (\hat{a} + \hat{a}^\dagger)^2 - \frac{1}{4Z_{LC}C_a} (\hat{a} - \hat{a}^\dagger)^2 \right] + \hat{H}_J + i \frac{1}{C_a} \left[C_s \hat{\Phi}(t, 0) - i \frac{C_s}{C_a} \sqrt{\frac{\hbar}{2Z_{LC}}} (\hat{a}^\dagger - \hat{a}) \right] \sqrt{\frac{\hbar}{2Z_{LC}}} [\hat{a}^\dagger - \hat{a}], \end{aligned} \quad (\text{S26})$$

where we used Heisenberg Eq. (S20) to eliminate \hat{Q}_1 . The last term inside the second parentheses contributes to the effective capacitance of the resonator, changing it to $C_p = C_a + C_s$. More rigorously: the choice $Z_{LC} = \sqrt{L_a/C_p}$ leads to the quadratic resonator part $(\hbar/\sqrt{L_a C_p}) \hat{a}^\dagger \hat{a} = \hbar \omega_a \hat{a}^\dagger \hat{a}$. Using the relation

$$\hat{\Phi}(0, t) = -i \sqrt{\frac{\hbar Z_0 \omega_a}{2}} [\hat{a}_{\text{in}}(t) + \hat{a}_{\text{out}}(t)], \quad (\text{S27})$$

the Heisenberg equations take the form

$$\hat{a}(t) = -i\bar{\omega}_a \hat{a}(t) + \frac{\alpha}{2} [\hat{a}_{\text{in}} + \hat{a}_{\text{out}}] + \frac{i}{\hbar} [\hat{H}_J, \hat{a}]. \quad (\text{S28})$$

Using $\hat{a}_{\text{out}}(t) - \hat{a}_{\text{in}}(t) = \alpha \hat{a}(t)$ and defining $\gamma_a = |\alpha|^2$ one arrives in the equation of motion

$$\hat{a}(t) = -i\bar{\omega}_a \hat{a}(t) - \frac{\gamma_a}{2} \hat{a}(t) - i\sqrt{\gamma_a} \hat{a}_{\text{in}} + \frac{i}{\hbar} [\hat{H}_J, \hat{a}]. \quad (\text{S29})$$

We would like to express the boundary condition and the equation of motion in a form used often in the literature. We do this by redefining the phase of the operators $\hat{a}_{\text{in}} \rightarrow -i\hat{a}_{\text{in}}$ and $\hat{a}_{\text{out}} \rightarrow i\hat{a}_{\text{out}}$, which leads to

$$\hat{a}(t) = -i\bar{\omega}_a \hat{a}(t) - \frac{\gamma_a}{2} \hat{a}(t) + \sqrt{\gamma_a} \hat{a}_{\text{in}} + \frac{i}{\hbar} [\hat{H}_J, \hat{a}] \quad (\text{S30})$$

$$\hat{a}_{\text{in}}(t) + \hat{a}_{\text{out}}(t) = \sqrt{\gamma_a} \hat{a}(t). \quad (\text{S31})$$

Similar Heisenberg equations can also be derived for the right-hand side transmission-line operators.

II. SINGLE-PHOTON INPUT

In this section, we derive the single-to-multi-photon scattering matrix given in the main part of the article. We also show how to linearize this problem and straightforwardly derive general results for the conversion probability. The linearization is possible in the case of a single incoming photon or weak coherent drive ($N_{\text{in}} \rightarrow 0$).

A. Scattering matrix

In the rotating-wave approximation, the coupling Hamiltonian between the two cavities has the form

$$\hat{H}_J = \hbar \epsilon_I \hat{a} \left(\hat{b}^\dagger \right)^n e^{-i\omega_J t} + \text{H.c.} \quad (\text{S32})$$

The Heisenberg equations of motion for the cavity fields are then

$$\frac{d}{dt} \hat{a}(t) = -i\omega_a \hat{a}(t) - \frac{\gamma_a}{2} \hat{a}(t) + \sqrt{\gamma_a} \hat{a}_{\text{in}}(t) - i\epsilon_I^* \left(\hat{b} \right)^n e^{+i\omega_J t} \quad (\text{S33})$$

$$\frac{d}{dt} \hat{b}(t) = -i\omega_b \hat{b}(t) - \frac{\gamma_b}{2} \hat{b}(t) + \sqrt{\gamma_b} \hat{b}_{\text{in}}(t) - i n \epsilon_I \hat{a} \left(\hat{b}^\dagger \right)^{n-1} e^{-i\omega_J t}. \quad (\text{S34})$$

1. Fourier transformed equations

For the present problem, we prefer to work with the Fourier-transformed Heisenberg equations of motion. The results derived using this method agree with the linearization technique introduced in the next section. Starting from the definitions

$$\hat{a}_{\text{in}}(t) = \frac{1}{\sqrt{2\pi}} \int d\omega \hat{a}_{\text{in}}(\omega) e^{-i\omega t} \quad (\text{S35})$$

$$\hat{a}_{\text{in}}(\omega) = \frac{1}{\sqrt{2\pi}} \int dt \hat{a}_{\text{in}}(t) e^{i\omega t}, \quad (\text{S36})$$

we get for the Heisenberg equations

$$F_a(\omega) \hat{a}(\omega) = \sqrt{\gamma_a} \hat{a}_{\text{in}}(\omega) - \bar{\epsilon}^* \int d\omega_1 \dots \int d\omega_{n-1} \hat{b}(\omega_1) \dots \hat{b}(\omega_{n-1}) \hat{b}(\omega + \omega_J - \omega_1 - \dots - \omega_{n-1}) \quad (\text{S37})$$

$$F_b(\omega) \hat{b}(\omega) = \sqrt{\gamma_b} \hat{b}_{\text{in}}(\omega) + n\bar{\epsilon} \int d\omega_1 \dots \int d\omega_{n-1} \hat{a}(\omega_1) \hat{b}^\dagger(\omega_2) \dots \hat{b}^\dagger(\omega_{n-1}) \hat{b}^\dagger(\omega_1 + \omega_J - \omega - \omega_2 - \dots - \omega_{n-1}),$$

where we have defined

$$F_{a/b}(\omega) = i(\omega_{a/b} - \omega) + \gamma_a/2 \quad (\text{S38})$$

$$\bar{\epsilon} = -i \frac{\epsilon_I}{(2\pi)^{(n-1)/2}}. \quad (\text{S39})$$

In these equations, the in-field $\hat{a}_{\text{in}}(\omega)$ [$\hat{b}_{\text{in}}(\omega)$] can be changed to out-field $-\hat{a}_{\text{out}}(\omega)$ [$-\hat{b}_{\text{out}}(\omega)$] with simultaneous change $\gamma_{a/b} \rightarrow -\gamma_{a/b}$ in $F_{a/b}(\omega)$ (obtained by using the resonator boundary conditions).

Our goal is to determine the amplitude (scattering matrix)

$$A = \left\langle 0 \left| \hat{b}_{\text{out}}(p_1) \hat{b}_{\text{out}}(p_2) \dots \hat{b}_{\text{out}}(p_n) \hat{a}_{\text{in}}^\dagger(k) \right| 0 \right\rangle, \quad (\text{S40})$$

with the help of resonator boundary conditions and Heisenberg equations of motion.

2. Scattering matrix in the case $n = 2$

We first consider in detail the case $n = 2$ and then describe the generalization to arbitrary n . Here, we evaluate the scattering element

$$\begin{aligned} A &= \left\langle 0 \left| \hat{b}_{\text{out}}(p_1) \hat{b}_{\text{out}}(p_2) \hat{a}_{\text{in}}^\dagger(k) \right| 0 \right\rangle \\ &= \left\langle 0 \left| \hat{b}_{\text{out}}(p_1) \hat{b}_{\text{out}}(p_2) \left[\sqrt{\gamma_a} \hat{a}^\dagger(k) - \hat{a}_{\text{out}}^\dagger(k) \right] \right| 0 \right\rangle. \end{aligned} \quad (\text{S41})$$

Since the out fields of different modes (by definition) need to commute, we must have

$$\left\langle 0 \left| \hat{b}_{\text{out}}(p_1) \hat{b}_{\text{out}}(p_2) \hat{a}_{\text{out}}^\dagger(k) \right| 0 \right\rangle = \left\langle 0 \left| \hat{b}_{\text{out}}(p_1) \hat{a}_{\text{out}}^\dagger(k) \hat{b}_{\text{out}}(p_2) \right| 0 \right\rangle = 0. \quad (\text{S42})$$

Therefore,

$$\left\langle 0 \left| \hat{b}_{\text{out}}(p_1) \hat{b}_{\text{out}}(p_2) \hat{a}_{\text{in}}^\dagger(k) \right| 0 \right\rangle = \sqrt{\gamma_a} \left\langle 0 \left| \hat{b}_{\text{out}}(p_1) \hat{b}_{\text{out}}(p_2) \hat{a}^\dagger(k) \right| 0 \right\rangle. \quad (\text{S43})$$

We then get

$$\begin{aligned} A &= \sqrt{\gamma_a} \left\langle 0 \left| \hat{b}_{\text{out}}(p_1) \hat{b}_{\text{out}}(p_2) \hat{a}^\dagger(k) \right| 0 \right\rangle \\ &= \frac{\gamma_a}{F_a(\omega_k)} \left\langle 0 \left| \hat{b}_{\text{out}}(p_1) \hat{b}_{\text{out}}(p_2) \left[\hat{a}_{\text{out}}^\dagger(k) + \frac{\bar{\epsilon}}{\sqrt{\gamma_a}} \int d\omega' \hat{b}^\dagger(\omega') \hat{b}^\dagger(\omega_k + \omega_J - \omega') \right] \right| 0 \right\rangle, \end{aligned} \quad (\text{S44})$$

where in the second form we used Eq. (S37). As the first term (inside the square brackets) again gives no contribution, we must have

$$A = \frac{\gamma_a}{F_a(\omega_k)} \frac{\bar{\epsilon}}{\sqrt{\gamma_a}} \int d\omega' \left\langle 0 \left| \hat{b}_{\text{out}}(p_1) \hat{b}_{\text{out}}(p_2) \hat{b}^\dagger(\omega') \hat{b}^\dagger(\omega_k + \omega_J - \omega') \right| 0 \right\rangle. \quad (\text{S45})$$

We continue by exploiting the Heisenberg equation

$$-F_b(\omega) \hat{b}^\dagger(\omega) = -\sqrt{\gamma_b} \hat{b}_{\text{out}}^\dagger(\omega) + 2 \times \bar{\epsilon}^* \int d\omega' \hat{a}^\dagger(\omega') \hat{b}(\omega' + \omega_J - \omega). \quad (\text{S46})$$

The factor 2 comes from the factor n in the boundary condition. When applying b to the ground state we obtain zero [since $b = (b_{\text{in}} + b_{\text{out}})/\sqrt{\gamma_b}$ and the ground state has no incoming or outgoing photons]. Therefore,

$$A = \frac{\gamma_a}{F_a(\omega_k)} \frac{\bar{\epsilon}}{\sqrt{\gamma_a}} \int d\omega' \left\langle 0 \left| \hat{b}_{\text{out}}(p_1) \hat{b}_{\text{out}}(p_2) \hat{b}^\dagger(\omega') \frac{\sqrt{\gamma_b}}{F_b(\omega_k + \omega_J - \omega')} \hat{b}_{\text{out}}^\dagger(\omega_k + \omega_J - \omega') \right| 0 \right\rangle. \quad (\text{S47})$$

In order to evaluate application by $b^\dagger(\omega')$, we again make use of the Heisenberg equation (S46). Consider first the term not proportional to $\bar{\epsilon}^*$, i.e., another multiplication by b_{out}^\dagger . Using

$$\langle 0|b(f_1)b(f_2)b^\dagger(f_3)b^\dagger(f_4)|0\rangle = \delta(f_1 - f_3)\delta(f_2 - f_4) + \delta(f_1 - f_4)\delta(f_2 - f_3), \quad (\text{S48})$$

we get for this term (we name it A_0),

$$A_0 = \bar{\epsilon} \frac{\sqrt{\gamma_a}}{F_a(\omega_k)} \left[\frac{\sqrt{\gamma_b}}{F_b(p_1)} \frac{\sqrt{\gamma_b}}{F_b(\omega_k + \omega_J - p_1)} + \frac{\sqrt{\gamma_b}}{F_b(p_2)} \frac{\sqrt{\gamma_b}}{F_b(\omega_k + \omega_J - p_2)} \right] \delta(\omega_k + \omega_J - p_1 - p_2) \quad (\text{S49})$$

$$= \bar{A}_0 \delta(\omega_k + \omega_J - p_1 - p_2). \quad (\text{S50})$$

The two terms inside the square brackets of Eq. (S49) are equal. This is the leading-order solution in $\bar{\epsilon}$.

The second contribution to A accounts for the non-perturbative limit. We need to evaluate

$$\begin{aligned} & - \int d\omega' f(\omega') \int d\omega'' \langle 0 | \hat{b}_{\text{out}}(p_1) \hat{b}_{\text{out}}(p_2) \hat{a}^\dagger(\omega'') \hat{b}(\omega'' + \omega_J - \omega') \hat{b}_{\text{out}}^\dagger(\omega_k + \omega_J - \omega') | 0 \rangle = \\ & - \int d\omega' f(\omega') \int d\omega'' \langle 0 | \hat{b}_{\text{out}}(p_1) \hat{b}_{\text{out}}(p_2) \hat{a}^\dagger(\omega'') \mathcal{I} \hat{b}(\omega'' + \omega_J - \omega') \hat{b}_{\text{out}}^\dagger(\omega_k + \omega_J - \omega') | 0 \rangle. \end{aligned} \quad (\text{S51})$$

Here we have defined

$$f(\omega') = 2 \times |\bar{\epsilon}|^2 \frac{\sqrt{\gamma_a}}{F_a(\omega_k)} \frac{\sqrt{\gamma_b}}{F_b(\omega_k + \omega_J - \omega')} \frac{1}{F_b(\omega')}. \quad (\text{S52})$$

In the second form we have also inserted identity operator \mathcal{I} between a^\dagger and b .

A crucial step here is based on the observation: only insertion $\mathcal{I} \rightarrow |0\rangle\langle 0|$ gives nonzero contribution. Similar property has also been used to evaluate scattering properties on a two-level system⁴⁴ and is possible due to photon-number conservation (here of the specific form $n_a + n_b/n = \text{constant}$). Eq. (S51) becomes then a product of two amplitudes. The left-hand side amplitude is proportional to A and the right-hand side amplitude measures scattering of single incoming photon from side b . Single incoming photon from side b has no change but to reflect at the junction in a way described by the solution for $\epsilon = 0$. This solution is derived in Section II B 1), where we get

$$\langle 0 | \hat{b}(p) \hat{b}_{\text{out}}^\dagger(k) | 0 \rangle = \frac{\sqrt{\gamma_b}}{F_b^*(\omega_k)} \delta(\omega_p - \omega_k). \quad (\text{S53})$$

Therefore, the term in Eq. (S51) can be rewritten in the form

$$- \frac{A}{\sqrt{\gamma_a}} \int d\omega' f(\omega') \frac{\sqrt{\gamma_b}}{F_b^*(\omega_k + \omega_J - \omega')}. \quad (\text{S54})$$

We then continue by evaluating the integration $\int d\omega'$ explicitly, which is done over the function

$$\begin{aligned} & -2|\epsilon|^2 A \frac{1}{F_a(\omega_k)} \frac{\sqrt{\gamma_b}}{F_b(\omega_k + \omega_J - \omega')} \frac{1}{F_b(\omega')} \frac{\sqrt{\gamma_b}}{F_b^*(\omega_k + \omega_J - \omega')} \\ & = - \frac{2|\epsilon|^2 A}{F_a(\omega_k)} \left| \frac{\sqrt{\gamma_b}}{\gamma_b/2 + i(\omega_k + \omega_J - \omega' - \omega_b)} \right|^2 \frac{1}{\gamma_b/2 + i(\omega_b - \omega')} \end{aligned}$$

Let us mark $\delta\omega = \omega_k + \omega_J - 2\omega_b$ (which is ideally zero). An analytical integration is possible and leads to the relation

$$A = A_0 - A \frac{1}{F_a(\omega_k)} \frac{4\pi|\bar{\epsilon}|^2}{\gamma_b + i\delta\omega}. \quad (\text{S55})$$

This means

$$A = \frac{A_0}{1 + a}, \quad a = 4\pi \frac{|\bar{\epsilon}|^2}{F_a(\omega_k)(\gamma_b + i\delta\omega)} = 2 \frac{|\epsilon_1|^2}{F_a(\omega_k)(\gamma_b + i\delta\omega)}. \quad (\text{S56})$$

where in the last form we went back to the original definition of $|\epsilon_1| = \sqrt{2\pi}|\bar{\epsilon}|$. The amplitude A_0 was derived

above,

$$A_0 = 2 \times \bar{\epsilon} \frac{\sqrt{\gamma_a}}{F_a(\omega_k)} \frac{\sqrt{\gamma_b}}{F_b(\omega_{p_1})} \frac{\sqrt{\gamma_b}}{F_b(\omega_k + \omega_J - \omega_{p_1} - \omega_{p_2})} \delta(\omega_k + \omega_J - \omega_{p_1} - \omega_{p_2}). \quad (\text{S57})$$

For the ideal case $\omega_k = \omega_a$ and $\delta\omega = 0$ we get

$$A = \frac{1}{1+a} \times 4 \frac{\bar{\epsilon}}{\sqrt{\gamma_a}} \frac{\gamma_b}{(\omega_b - \omega_{p_1})^2 + \gamma_b^2/4} \delta(2\omega_b - \omega_{p_1} - \omega_{p_2}) \quad , \quad a = \frac{4|\epsilon_I|^2}{\gamma_a \gamma_b}. \quad (\text{S58})$$

To find the multiplication probability, we evaluate the photon number on side b . This means evaluating

$$P = \int d\omega \int d\omega' \langle 1_a | \hat{b}_{\text{out}}^\dagger(\omega) \hat{b}_{\text{out}}(\omega') | 1_a \rangle. \quad (\text{S59})$$

The trick here is to insert a single- b -side-photon state in between the two operators (based on the same observation as made when calculating Eq. [S51]),

$$P = \int d\omega \int d\omega' \int d\omega'' \langle 1_a | \hat{b}_{\text{out}}^\dagger(\omega) | 1_{b\omega''} \rangle \langle 1_{b\omega''} | \hat{b}_{\text{out}}(\omega') | 1_a \rangle, \quad (\text{S60})$$

which means that the photon number has the form

$$P = \frac{1}{(1+a)^2} \int d\omega_{p_1} |\bar{A}_0(\omega_{p_1}, \omega_k - \omega_{p_1})|^2. \quad (\text{S61})$$

Here $\bar{A}_0(\omega_{p_1}, \omega_{p_2})$ was defined to be the same as A_0 but without the delta-function, Eq. (S50). The integration is over a product of two Lorentzian functions and can again be performed analytically. For the ideal case $\omega_k = \omega_a$ and $\delta\omega = 0$ we get

$$P = 2 \times \frac{4a}{(1+a)^2}, \quad (\text{S62})$$

which is the final result.

Scattering matrix for general n

Let us discuss now how the previous derivation is modified in the case of general n . In this situation, Eq. (S48) gets generalized to $n!$ identical contributions, leading to the leading-order amplitude

$$A_0 = n! \times \bar{\epsilon} \frac{\sqrt{\gamma_a}}{F_a(\omega_k)} \frac{\sqrt{\gamma_b}}{F_b(p_1)} \dots \frac{\sqrt{\gamma_b}}{F_b(p_n)} \delta(\omega_k + \omega_J - p_1 - \dots - p_n). \quad (\text{S63})$$

Eq. (S46) includes a factor n instead of the factor 2. Applying this equation to solve Eq. (S51), we get a higher-order contribution in $\bar{\epsilon}$ only when the last of the creations by \hat{b}^\dagger is replaced by $n \times \hat{a}^\dagger(\tilde{\omega}_1) \hat{b}(\tilde{\omega}_2) \dots \hat{b}(\tilde{\omega}_{n-1}) \hat{b}(\tilde{\omega}_1 + \omega_J - \omega_1 - \tilde{\omega}_2 - \dots - \tilde{\omega}_{n-1})$. The other terms (on the right-hand side of this) contribute with the zeroth-order term, $\hat{b}_{\text{out}}^\dagger(\omega_2) \dots \hat{b}_{\text{out}}^\dagger(\omega_{n-1}) \hat{b}_{\text{out}}^\dagger(\omega_k + \omega_J - \omega_1 - \dots - \omega_{n-1})$. This leads to the general form of the function

$$f(\omega') \rightarrow f(\omega_1, \dots, \omega_{n-1}) = n \times |\bar{\epsilon}|^2 \frac{\sqrt{\gamma_a}}{F_a(\omega_k)} \frac{1}{F_b(\omega_1)} \frac{\sqrt{\gamma_b}}{F_b(\omega_2)} \dots \frac{\sqrt{\gamma_b}}{F_b(\omega_k + \omega_J - \omega_1 - \dots - \omega_{n-1})}. \quad (\text{S64})$$

Eq. (S51) is then again a product of two amplitudes. The left-hand side amplitude is proportional to A and the right-hand side amplitude measures scattering of $n-1$ incoming photons from side b . The (left-hand side) factor A has now been evaluated with respect to final state $\tilde{\omega}_1$. Again, $n-1$ incoming photon from side b has no change but to reflect at the junction in a way described by the solution for $\epsilon = 0$. We can then evaluate the (right-hand side) expectation value

$$E = \left\langle \hat{b}(\tilde{\omega}_2) \dots \hat{b}(\tilde{\omega}_{n-1}) \hat{b}(\tilde{\omega}_1 + \omega_J - \omega_1 - \tilde{\omega}_2 - \dots - \tilde{\omega}_{n-1}) \times \hat{b}_{\text{out}}^\dagger(\omega_2) \dots \hat{b}_{\text{out}}^\dagger(\omega_{n-1}) \hat{b}_{\text{out}}^\dagger(\omega_k + \omega_J - \omega_1 - \dots - \omega_{n-1}) \right\rangle,$$

by using the relation between \hat{b} and \hat{b}_{out} obtained for $\bar{\epsilon} = 0$ (Section II B 1), which gives

$$\int d\tilde{\omega}_1 \dots d\tilde{\omega}_{n-1} E = (n-1)! \frac{\sqrt{\gamma_b}}{F_b^*(\omega_2)} \dots \frac{\sqrt{\gamma_b}}{F_b^*(\omega_k + \omega_J - \omega_1 - \dots - \omega_{n-1})}, \quad (\text{S65})$$

and $\tilde{\omega}_1 = \omega_k$ in the (left-hand side) matrix element corresponding to amplitude A . The last step is then to evaluate the integral

$$\frac{A}{F_a(\omega_k)} |\bar{\epsilon}|^2 n \times (n-1)! \int d\omega_1 \dots d\omega_{n-1} \left| \frac{\sqrt{\gamma_b}}{F_b(\omega_2)} \right|^2 \dots \left| \frac{\sqrt{\gamma_b}}{F_b(\omega_k + \omega_J - \omega_1 - \dots - \omega_{n-1})} \right|^2 \times \frac{1}{F_b(\omega_1)}, \quad (\text{S66})$$

The evaluation can again be done analytically and gives the result

$$\frac{A |\bar{\epsilon}|^2}{F_a(\omega_k)} \frac{2n! (2\pi)^{n-1}}{n\gamma_b - 2i\delta\omega}. \quad (\text{S67})$$

This leads us to the result in the ideal case $\delta\omega = 0$, $\omega_k = 0$,

$$A = \frac{A_0}{1+a}, \quad a = 4 \frac{(n-1)! |\epsilon_I|^2}{\gamma_a \gamma_b}. \quad (\text{S68})$$

In the more general form we have

$$a = \frac{1}{F_a(\omega_k)} \frac{2n! |\epsilon_I|^2}{n\gamma_b - 2i\delta\omega}. \quad (\text{S69})$$

The photon number on side b is evaluated similarly as in the case $n = 2$, by inserting a state $(1/\sqrt{(n-1)!}) \int d\omega_1 \dots d\omega_{n-1} \hat{b}_{\text{out}}^\dagger(\omega_1) \dots \hat{b}_{\text{out}}^\dagger(\omega_{n-1}) |0\rangle$ between the operators in the expectation value of Eq. (S59). The result for the photon number on side b for general n agrees with the result from the linearization method described below.

B. Linearization approach

If we are only interested in the probability of multiplication, and not in the exact form of the frequency correlations, we can solve the problem straightforwardly with proper linearization approach. The results derived here agree with the scattering-matrix approach introduced in Section II A, which is also able to capture the frequency correlations.

1. Decoupled resonators ($E_J = 0$)

Consider first the case $\epsilon_I = 0$ ($E_J = 0$), i.e., when resonator a is decoupled from resonator b . Considering incoming radiation from the transmission line a , we only need to solve the equation

$$\dot{\hat{a}}(t) = -i\omega_a \hat{a}(t) - \frac{\gamma_a}{2} \hat{a}(t) + \sqrt{\gamma_a} \hat{a}_{\text{in}}(t). \quad (\text{S70})$$

A Fourier transformation gives

$$-i\omega \hat{a}(\omega) = -i\omega_a \hat{a}(\omega) - \frac{\gamma_a}{2} \hat{a}(\omega) + \sqrt{\gamma_a} \hat{a}_{\text{in}}(\omega). \quad (\text{S71})$$

The solution for the resonator field is then

$$\hat{a}(\omega) = \frac{\sqrt{\gamma_a}}{i(\omega_a - \omega) + \frac{\gamma_a}{2}} \hat{a}_{\text{in}}(\omega), \quad (\text{S72})$$

whereas the out-field has the form

$$\hat{a}_{\text{out}}(\omega) = \frac{\frac{\gamma_a}{2} - i(\omega_a - \omega)}{\frac{\gamma_a}{2} + i(\omega_a - \omega)} \hat{a}_{\text{in}}(\omega). \quad (\text{S73})$$

Similar relations are also valid for the propagating fields in the transmission line b . This result states that all incoming radiation will be reflected with a specific phase shift. At resonance ($\omega = \omega_a$) we have $\hat{a}(\omega) = (2/\sqrt{\gamma_a})\hat{a}_{\text{in}}(\omega)$, which means that in the relation $\hat{a}_{\text{out}}(\omega) = \sqrt{\gamma_a}\hat{a}(\omega) - \hat{a}_{\text{in}}(\omega)$ the contribution from the cavity is exactly twice the incoming field. On the other hand, in the case $\epsilon_I \neq 0$, we aim for the opposite situation, where these two contributions cancel each other and there will be no reflection.

Note that in the original definition of the annihilation and creation operators we have a minus sign difference between the in- and out-fields (see Sec. I). This means that we actually have a " π -shift" in the amplitude when $\omega = \omega_a$. In our system, the phase shift plays no role on the described effects. However, this can play an important role in other systems, for example in a microwave reflection on a Transmon qubit connected to two semi-infinite transmission lines [48].

2. Solution for linear conversion ($n = 1$)

We consider now the case $\epsilon_I \neq 0$ but $n = 1$, which also allows for straightforward analytical solution. After Fourier transformation our equations get the form

$$-i\omega\hat{a}(\omega) = -i\omega_a\hat{a}(\omega) - \frac{\gamma_a}{2}\hat{a}(\omega) + \sqrt{\gamma_a}\hat{a}_{\text{in}}(\omega) - \bar{\epsilon}^*\hat{b}(\omega + \omega_J) \quad (\text{S74})$$

$$-i\omega\hat{b}(\omega) = -i\omega_b\hat{b}(\omega) - \frac{\gamma_b}{2}\hat{b}(\omega) + \sqrt{\gamma_b}\hat{b}_{\text{in}}(\omega) + \bar{\epsilon}\hat{a}(\omega - \omega_J). \quad (\text{S75})$$

A solution is

$$\hat{b}(\omega) \left[-i\omega + i\omega_b + \frac{\gamma_b}{2} + \frac{|\bar{\epsilon}|^2}{i(\omega_a - \omega + \omega_J) + \frac{\gamma_a}{2}} \right] = \sqrt{\gamma_b}\hat{b}_{\text{in}}(\omega) + \frac{\bar{\epsilon}\sqrt{\gamma_a}\hat{a}_{\text{in}}(\omega - \omega_J)}{i(\omega_a - \omega + \omega_J) + \frac{\gamma_a}{2}}. \quad (\text{S76})$$

We assume now that there is no input from side b . In this case, the outgoing photon flux to side b can be deduced from

$$\langle \hat{b}_{\text{out}}^\dagger(\omega)\hat{b}_{\text{out}}(\omega') \rangle = \gamma_b \langle \hat{b}^\dagger(\omega)\hat{b}(\omega') \rangle = \frac{\gamma_a\gamma_b|\bar{\epsilon}|^2}{||\bar{\epsilon}|^2 + F_a(\omega - \omega_J)F_b(\omega)}^2 \langle \hat{a}_{\text{in}}^\dagger(\omega - \omega_J)\hat{a}_{\text{in}}(\omega' - \omega_J) \rangle, \quad (\text{S77})$$

where make use of the fact that for a single-photon input only $\omega = \omega'$ contributes. For the following formulas, we make the shift $\omega - \omega_J \rightarrow \omega$.

We then obtain the transmission probability

$$P = \frac{\gamma_a\gamma_b|\bar{\epsilon}|^2}{||\bar{\epsilon}|^2 + F_a(\omega)F_b(\omega + \omega_J)|^2}. \quad (\text{S78})$$

When $\omega = \omega_a$ and $\omega + \omega_J = \omega_b$, we obtain

$$P = \frac{4a}{(1+a)^2}, \quad (\text{S79})$$

where $a = 4\epsilon_I^2/\gamma_a\gamma_b$. Perfect conversion occurs when $a = 1$. This demonstrates that a Josephson junction can also be used for bare frequency conversion ($n = 1$).

When $\omega = \omega_a$ and $\omega + \omega_J = \omega_b + \delta\omega$ (describing the effect of bias voltage offset), we obtain

$$P = \frac{4a}{(1+a)^2 + \frac{4\delta\omega^2}{\gamma_b^2}}. \quad (\text{S80})$$

We see that voltage offset decreases the conversion probability. In the case $a = 1$ we have $P = 1/(1 + \delta\omega^2/\gamma_b^2)$.

3. Multiplication by arbitrary n

Consider photon multiplication by a factor $n > 1$. We make now an important observation: In the case of single incoming photon, the resonators can be analytically treated as two-level systems. The reason is that when the photon

number of resonator b drops from n to $n - 1$, there is no way for the resonator a to be repopulated: the remaining $n - 1$ photons in resonator b will inevitable be dissipated in the transmission line b . The effective decay rate of the excited state of the two-level system b is then the one from the state n to the state $n - 1$, that is $\tilde{\gamma}_b = n\gamma_b$. Similarly, the effective coupling between the two-level systems is $\tilde{\epsilon}_I = \epsilon_I\sqrt{n!}$. The final equations of motion are linear and the above solution is valid. The photon multiplication probability is then

$$P = \frac{\gamma_a \tilde{\gamma}_b |\tilde{\epsilon}|^2}{\left| |\tilde{\epsilon}|^2 + F_a(\omega) \tilde{F}_b(\omega + \omega_J) \right|^2}, \quad (\text{S81})$$

where $\tilde{F}_b(\omega)$ is evaluated using the decay $\tilde{\gamma}_b = n\gamma_b$. In the ideal case $\omega = \omega_a$, $\omega + \omega_J = \omega_b$ we get

$$P = \frac{1}{n} \frac{\langle \hat{b}_{\text{out}}^\dagger(t) \hat{b}_{\text{out}}(t) \rangle}{\langle \hat{a}_{\text{in}}^\dagger(t) \hat{a}_{\text{in}}(t) \rangle} = \frac{4\tilde{a}}{(1 + \tilde{a})^2} \quad (\text{S82})$$

$$\tilde{a} = 4 \frac{|\epsilon_I|^2 (n-1)!}{\gamma_a \gamma_b}. \quad (\text{S83})$$

For a general bias voltage offset $\delta\omega$ (see above) we get

$$P = \frac{4\tilde{a}}{(1 + \tilde{a})^2 + \frac{4\delta\omega^2}{n^2\gamma_b^2}}. \quad (\text{S84})$$

In the case $a = 1$ we have $P = 1/(1 + \delta\omega^2/n^2\gamma_b^2)$.

4. Multiplier bandwidth

The input bandwidth of the multiplier can be deduced by setting $\omega = \omega_a + \delta\omega$ and $\omega + \omega_J = \omega_b + \delta\omega$. This gives

$$P = \frac{4\tilde{a}}{(1 + \tilde{a})^2 + 4 \left(\frac{\delta\omega(\gamma_a + \tilde{\gamma}_b)}{\gamma_a \tilde{\gamma}_b} \right)^2 - 16\tilde{a} \frac{\delta\omega^2}{\gamma_a \tilde{\gamma}_b} + 16 \left(\frac{\delta\omega^2}{\gamma_a \tilde{\gamma}_b} \right)^2}. \quad (\text{S85})$$

In the case $\tilde{a} = 1$ we get

$$P = \frac{1}{1 + x^2 \frac{(n+1)^2}{n^2} - 4 \frac{x^2}{n} + 4 \frac{x^4}{n^2}} = \frac{1}{1 + x^2 \left(1 - \frac{1}{n}\right)^2 + 4 \frac{x^4}{n^2}}, \quad (\text{S86})$$

where we defined $x = \delta\omega/\gamma_a$ and assumed $\gamma_b = \gamma_a$. The limiting cases are $P = 1/(1+4x^4)$ for $n = 1$ and $P = 1/(1+x^2)$ for large n . The full width at half maximum changes here from γ ($n = 1$) to 2γ ($n \gg 1$).

III. MULTI-PHOTON INPUT

In this section, we generalize the Hamiltonian of the Josephson junction to also to account for multi-photon populations in the resonator a , and show how to model the resulting resonator dynamics within density-matrix formalism in the case of an incoming coherent state. After this additional numerical results on photon multiplication properties in alternative parameter regimes are shown.

A. Generalized Josephson Hamiltonian

The general form of the Josephson Hamiltonian can be deduced from the following form of the matrix elements between resonator Fock states,

$$\left\langle s \left| e^{ig\hat{a}+ig\hat{a}^\dagger} \right| t \right\rangle = e^{-g^2/2} (i)^{s-t} \sqrt{\frac{t!}{(s)!}} L_t^{(s-t)}(g^2), \quad (\text{S87})$$

where $L_i^{(j)}(x)$ is the Laguerre polynomial. We apply this for the Josephson Hamiltonian $\hat{H}_J = -E_J \cos \left[\omega_J + g_a(\hat{a} + \hat{a}^\dagger) - g_b(\hat{b} + \hat{b}^\dagger) \right]$ assuming $\omega_J + \omega_a \approx n\omega_b$ and using the rotating-wave approximation. This gives

$$\hat{H}_J^{\text{RWA}} = -\frac{E_J}{2} \sum_{k=0}^{\infty} (i)^n A_{k+n,k}(g_b) |k+n\rangle_b \langle k|_b \times \sum_{l=0}^{\infty} (-i) A_{l+1,l}(g_a) |l\rangle_a \langle l+1|_a e^{-i\omega_J t} + \text{H.c.}, \quad (\text{S88})$$

where the $|n\rangle_{a/b}$ refers to the Fock state n of resonator a/b and

$$A_{k+n,k}(g) = g^n e^{-g^2/2} \sqrt{\frac{k!}{(k+n)!}} L_k^{(n)}(g^2). \quad (\text{S89})$$

B. Master-equation approach

A coherent state as an input state appears as a complex number in the Heisenberg equations for averages. From these equations we can then deduce the equivalent Lindblad-type master equation.

For example, if we assume an incoming coherent state in the transmission line a and write $\langle \hat{a}_{\text{in}}(t) \rangle = \epsilon(t)$, by taking expectation value over the initial (product) state (in the far past), we get the equations of motion for the expectation values

$$\begin{aligned} \epsilon(t) + \langle \hat{a}_{\text{out}}(t) \rangle &= \sqrt{\gamma_a} \langle \hat{a}(t) \rangle \\ \langle \hat{b}_{\text{out}}(t) \rangle &= \sqrt{\gamma_b} \langle \hat{b}(t) \rangle \\ \frac{d}{dt} \langle \hat{a}(t) \rangle &= -i\omega_a \langle \hat{a}(t) \rangle - \frac{\gamma_a}{2} \langle \hat{a}(t) \rangle + \sqrt{\gamma_a} \epsilon(t) - i\epsilon_1^* \left\langle \left(\hat{b} \right)^n \right\rangle e^{+i\omega_J t} \\ \frac{d}{dt} \langle \hat{b}(t) \rangle &= -i\omega_b \langle \hat{b}(t) \rangle - \frac{\gamma_b}{2} \langle \hat{b}(t) \rangle - in\epsilon_1 \left\langle \hat{a} \left(\hat{b}^\dagger \right)^{n-1} \right\rangle e^{-i\omega_J t}. \end{aligned} \quad (\text{S90})$$

Similarly, we can construct equations of motion for averages of operators $\hat{a}^\dagger(t)\hat{a}(t)$, $\hat{b}^\dagger(t)\hat{b}(t)$, and so on.

From equations of motion for averages, we can deduce the equivalent Lindblad-type master equation. In this formulation, we have a total Hamiltonian $\hat{H} = \hat{H}_0 + \hat{H}_J + \hat{H}_d$, where the incoming radiation from side a takes the form of a classical drive,

$$\hat{H}_d = -i\hbar\sqrt{\gamma_a}\epsilon^*(t)\hat{a} + i\hbar\sqrt{\gamma_a}\epsilon(t)\hat{a}^\dagger. \quad (\text{S91})$$

The final equation of motion has the form

$$\dot{\hat{\rho}} = i[\hat{\rho}, \hat{H}] + \mathcal{L}_a[\hat{\rho}] + \mathcal{L}_b[\hat{\rho}], \quad (\text{S92})$$

where $\hat{\rho}$ is the full two-oscillator density matrix and the Lindblad super-operator \mathcal{L}_a describes decay of field of the oscillator a to the left-hand side transmission line, defined as

$$\mathcal{L}_a[\hat{\rho}] = \frac{\gamma_a}{2} (2\hat{a}\hat{\rho}\hat{a}^\dagger - \hat{a}^\dagger\hat{a}\hat{\rho} - \hat{\rho}\hat{a}^\dagger\hat{a}), \quad (\text{S93})$$

and similarly for $\mathcal{L}_b[\hat{\rho}]$.

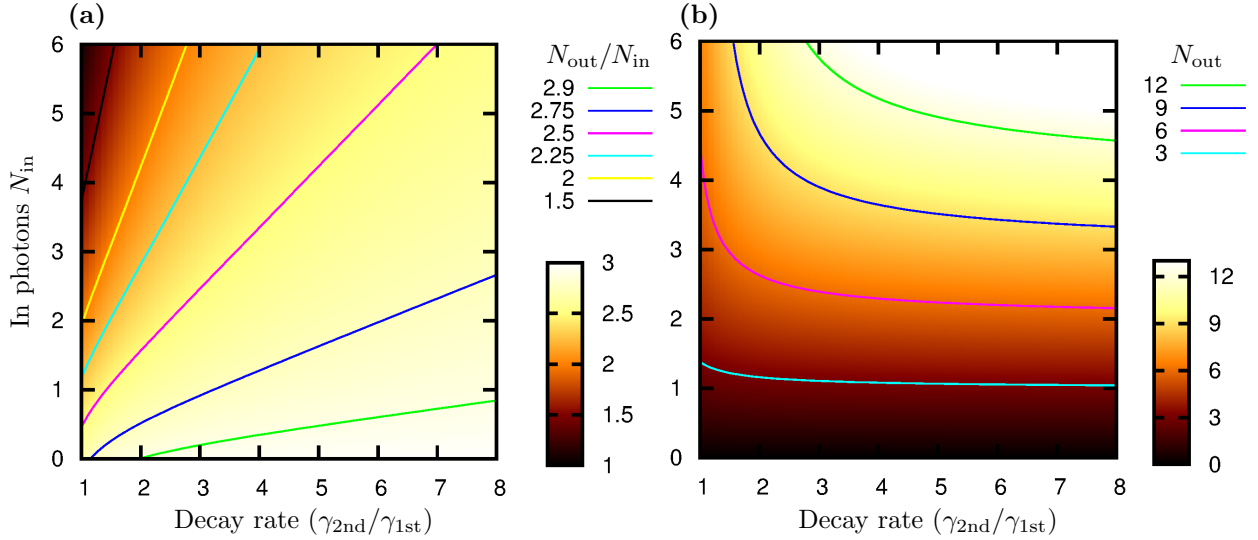


FIG. S2: (a): The multiplication factor N_{out}/N_{in} for $g_a = g_b = 1$ as a function of cavity decay rate γ_{2nd} and average input photon number N_{in} when biased at the photon-tripling resonance ($n = 3$). We have $\gamma_a = \gamma_b$ and $|\epsilon_n| = 2\sqrt{2}\epsilon_I/\gamma = 1$. (b): The average number of created photons in the same simulation.

C. Additional numerical results

Here, we analyze further numerical results obtained by using the master-equation approach. We consider first replotting the data of Fig. 2 in the main part of the article, in the Supplemental Material shown as Fig. S2(a), in a way where the actual number of created photons is explicit, see Fig. S2(b). In detail, we find that two input photons and three times larger second-stage bandwidth ($\gamma_{2nd}/\gamma_{1st} = 3$) produce on average 5 photons. The outgoing wavepacket has in a good approximation the same form as the incoming one (not plotted). We can then estimate the effect of a third multiplication within the same plot by using the input $N_{in} = 5$. Using the same bandwidth raises the average photon beyond $N_{out} = 10$.

In Fig. S3(a), we plot the multiplication efficiency by reducing $g_a \rightarrow 0.25$ and keeping $g_b = 1$. We find that the multiplication efficiency gets better for larger input numbers, which is naturally a very positive result. However, to achieve $|\epsilon_n| = 1$, the tradeoff is that here we need larger E_J , and this increases the emission without input roughly by a factor $1/g_a^2 = 16$, see Section V C. Furthermore, by increasing g_b and keeping $g_a = 0.25$, we find even better multiplication efficiency (not plotted) and at the same time reduced spurious emission if compared to $g_a = 0.25$ and $g_b = 1$. Understanding physics in this (experimentally more challenging) parameter range is very interesting for further theoretical work.

In Fig. S3(b), we study the multiplication efficiency as a function of resonator coupling $|\epsilon_n|$. The simulations are made again with $\gamma_a = \gamma_b \equiv \gamma$. We modify $|\epsilon_n|$ around the optimal value 1, which corresponds to $|\epsilon_I| = 2\sqrt{2}\gamma$. Bandwidths are kept constant, so we are basically tuning only E_J . We see that the optimal value for $|\epsilon_n|$ stays surprisingly close to $|\epsilon_n| = 1$ also for increased photon numbers. Here, slight increase of $|\epsilon_n|$ can be used to slightly increase the multiplication efficiency for larger average photon numbers.

IV. POST AMPLIFICATION AND SINGLE-PHOTON DETECTION

Our photo multiplier can be transformed into a single photon detector by placing a quantum limited (phase preserving) amplifier at the output of the photo-multiplier. The output of a phase-preserving quantum limited amplifier is the scaled Husimi Q function of its input⁴⁹:

$$Q_{out}(\alpha) = \frac{1}{G} Q_{in}(\alpha/\sqrt{G}). \quad (S94)$$

When the amplifier gain G is large, so that commutators at the output can be neglected, $Q_{out}(\alpha)$ directly describes the classical probability density to observe a classical complex amplitude α at the output.

For a single-photon input of the photomultiplier with gain n we get a n photon Fock state at the input of the

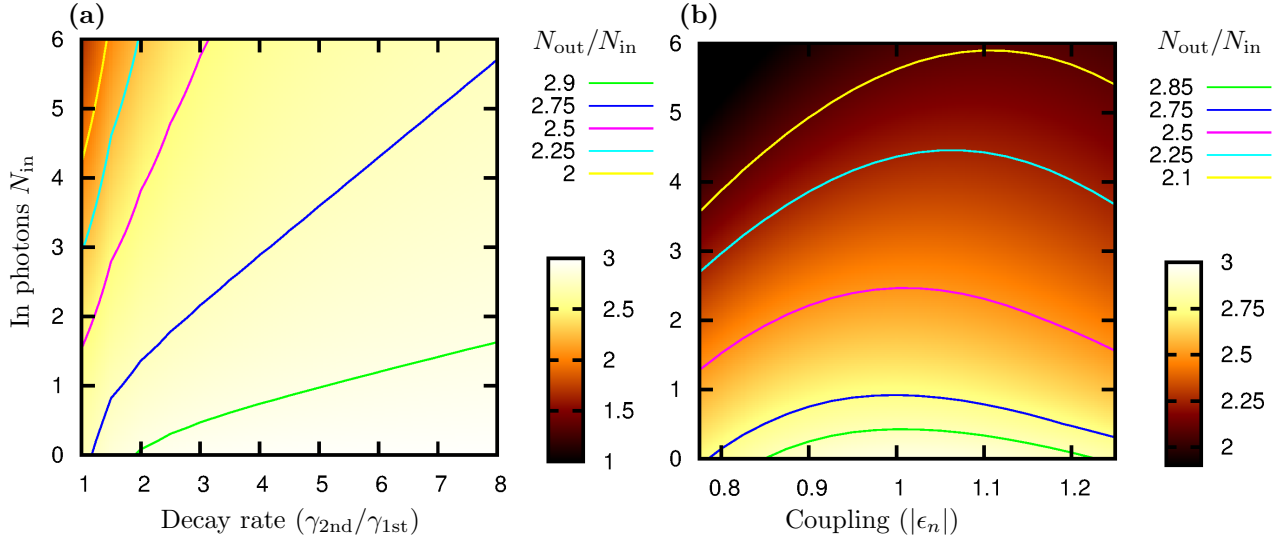


FIG. S3: (a): The multiplication factor $N_{\text{out}}/N_{\text{in}}$ for $g_a = 0.25$ and $g_b = 1$ as a function of cavity decay rate $\gamma_{2\text{nd}}$ and average input photon number N_{in} when biased at the photon-tripling resonance ($n = 3$). We have $\gamma_a = \gamma_b$ and $|\epsilon_n| = 2\sqrt{2}\epsilon_I/\gamma = 1$. The multiplication of higher photon numbers is better than for $g_a = g_b = 1$. The tradeoff of is stronger emission without input. (b): The multiplication factor when the resonator coupling ϵ_n is tuned away from $\epsilon_n = 1$ for $g_a = g_b = 1$. The maximal efficiency is here close to $|\epsilon_n| = 1$ also for increased photon number, but can be enhanced by properly tuning ϵ_n (E_J).

amplifier, with a Husimi function $Q_{\text{in},n}(\alpha)$ independent of the phase of α . In order to read the output of the photo-multiplier we detect (or calculate) the output power $|\alpha|^2$. We suppose here that the amplifier has the same bandwidth as the photo-multiplier, γ , or that it has a wider bandwidth but only the output power in the output bandwidth of the photo-multiplier is considered. In order to make the following calculations independent of the gain of the amplifier, we consider the average input photon number per bandwidth $|\alpha|^2/(\gamma G)$, calculated from the classical output amplitude α .

The distribution $D_n(N)$ of measured effective photon number N for n photon input to the amplifier is:

$$D_n(N) = \pi Q_{\text{in},n}(\sqrt{N}) = \frac{N^n}{n!} e^{-N}. \quad (\text{S95})$$

In order to discriminate between a photon and no-photon, we set a threshold N_{th} , with lower powers being interpreted as ‘no click’ and higher powers as ‘click’. The probability to get a false click during an inverse bandwidth is:

$$P_{\text{dark}} = \int_{N_{\text{th}}}^{\infty} dN D_0(N), \quad (\text{S96})$$

and the probability to miss a n -photon Fock state at the input of the amplifier is

$$P_{\text{miss}} = \int_0^{N_{\text{th}}} dN D_n(N). \quad (\text{S97})$$

The resulting dark-count probability and the probability of missed photon as a function of chosen threshold are plotted in the main part of the article, in Fig. 3.

V. IMPERFECTIONS

In this section, we describe in more detail our theory that estimates the effect of finite temperature to conversion probability and photon emission rate in the absence of input radiation (spontaneous emission).

A. Effect of thermal fluctuations

We assume that the voltage fluctuations manifest themselves by a low-frequency drifting of the junction voltage. To study the effect of the fluctuations, we first solve the steady state conversion for $\omega_a + \omega_J \neq n\omega_b$ (keeping $\omega_{\text{in}} = \omega_a$). Such a conversion is described by a Lorentzian, Eq. (S84), relating the incoming and outgoing photon fluxes,

$$\frac{f_{\text{out}}(\delta\omega_J)}{f_{\text{in}}} = n \frac{(n\gamma_b)^2}{(n\gamma_b)^2 + \delta\omega^2},$$

where $\delta\omega = \omega_J - (n\omega_b - \omega_a)$.

On the other hand, the probability distribution of the values for fluctuating voltage, which we call $P_{\text{f}}(\hbar\delta\omega_J)$, is in a good approximation a Lorentzian with linewidth $\gamma_{\text{th}} = 2\pi k_B T Z_0 / R_Q \hbar$, where Z_0 is the low-frequency impedance,

$$P_{\text{f}}(\hbar\delta\omega_J) \approx \frac{1}{\hbar} \frac{1}{\pi} \frac{\gamma_{\text{th}}}{\gamma_{\text{th}}^2 + \omega_J^2}. \quad (\text{S98})$$

This can be derived, for example, by applying the so-called $P(E)$ -theory for a low-Ohmic environment¹⁶.

Putting the above observations together, we find an approximative result for the average reflection probability of an incoming photon of frequency $\omega_{\text{in}} = \omega_a$,

$$P_{\text{reflection}} \approx 1 - \int_{-\infty}^{\infty} d\delta\omega \frac{(n\gamma_b)^2}{(n\gamma_b)^2 + \delta\omega^2} P_{\text{f}}(\hbar\delta\omega) = 1 - \frac{n\gamma_b}{\gamma_{\text{th}} + n\gamma_b} = \frac{\gamma_{\text{th}}}{\gamma_{\text{th}} + n\gamma_b}. \quad (\text{S99})$$

B. Limitations set by experimental feasibility

The result of Eqs. (S82-S83) implies that any photon number n can be generated from a single-photon input by correctly tuning ϵ_{I} . However, terms beyond the rotating-wave approximation have been neglected and need to be considered carefully. It turns out that strong higher-order processes practically demand strong couplings g_i , as expected. In a typical experiment we have $g_i \sim 0.2$ and multi-photon emission is weak^{19–21}. Presently, values $g_i = 1$ and slightly beyond can be achieved, for example, by building resonators from high kinetic inductance materials or Josephson junction arrays⁵⁰.

If we consider the experimentally feasible situation $g_{a/b} = 1$ and choose $\gamma_a = \gamma_b = \gamma$, for a reflectionless multiplication with n we need a Josephson coupling energy

$$\frac{E_J^*}{\hbar\gamma} = \frac{n!}{\sqrt{(n-1)!}}, \quad (\text{S100})$$

where $E_J^* = e^{-g_a^2/2 - g_b^2/2} E_J$ accounts for the renormalization of E_J . We see that the value for E_J increases rapidly with n , the first right-hand side numbers being 1, 2, 4.2, 9.8, 24.5, ... Two important effects increase with E_J due to non-RWA terms: (i) emission without incoming radiation and (ii) reflection of incoming radiation.

C. Emission without input

The most dangerous effect from terms beyond the rotating-wave approximation is the emission without incoming microwave radiation. Assuming that this effect is weak, we can estimate the photon flux density by using the perturbative method developed in Refs. [21,25,26]. This gives for the photon flux density

$$f(\omega) = \frac{1}{2\pi} \int d\omega' \langle a^\dagger(\omega) a(\omega') \rangle = \sum_{\pm} \frac{I_c^2 \text{Re}[Z_{\text{t}}(\omega)]}{2\omega} P[\hbar(\pm\omega_J - \omega)]. \quad (\text{S101})$$

Here the probability density $P(E)$ has the form¹⁶

$$P(E) = \int_{-\infty}^{\infty} dt \frac{1}{2\pi\hbar} e^{J(t)} e^{i\frac{E}{\hbar}t}, \quad (\text{S102})$$

where the phase-correlation function depends on the impedance seen by the tunnel junction, $Z_t(\omega)$, as

$$J(t) = \left\langle \left[\hat{\phi}_0(t) - \hat{\phi}_0(0) \right] \hat{\phi}_0(0) \right\rangle \quad (\text{S103})$$

$$\left\langle \hat{\phi}_0(t) \hat{\phi}_0(t') \right\rangle = 2 \int_{-\infty}^{\infty} \frac{d\omega}{\omega} \frac{\text{Re}[Z_t(\omega)]}{R_Q} \frac{e^{-i\omega(t-t')}}{1 - e^{-\beta\hbar\omega}}. \quad (\text{S104})$$

The two signs in Eq. (S101) correspond to forward (+) and backward (-) Cooper-pair tunneling events. This is an optimal way of determining emission flux in the weak perturbation limit, i.e., when the emission rate is much smaller than the resonator decay rates.

Similarly, the photon flux in the presence of a coherent input can be deduced to be

$$\frac{1}{2\pi} \int d\omega' \langle a^\dagger(\omega) a(\omega') \rangle = \sum_{\pm} \sum_{m=-\infty}^{\infty} \frac{I_c^2 \text{Re}[Z_t(\omega)]}{2\omega} P[\hbar(\pm\omega_J - \omega + m\omega_0)] |J_m(a)|^2. \quad (\text{S105})$$

Photons can be absorbed from ($m > 0$) or emitted into ($m < 0$) the drive beam. The dimensionless amplitude a characterizes phase fluctuations induced by the drive at frequency ω_0 . This function will only be used here to visualize the strength of the conversion rate versus the emission without input rate.

As environmental (tunnel) impedance we consider an impedance with Lorentzian resonance at frequency ω_b

$$\text{Re}[Z_t(\omega)] = \frac{1}{C} \frac{\gamma_b}{1 + 4(\omega - \omega_b)^2 \gamma_b^2} \approx \frac{\pi}{2C} \delta(\omega - \omega_b). \quad (\text{S106})$$

At zero temperature and in the limit $\gamma_b \rightarrow 0$ this leads to¹⁶

$$P(E) = e^{-\rho_b} \sum_{n=0}^{\infty} \frac{\rho_b^n}{n!} \delta(E - n\hbar\omega_b). \quad (\text{S107})$$

We have defined here $\rho_b = (4e^2/2C)/\hbar\omega_b$. The connection to the previously used parameters is

$$\rho_b = g_b^2. \quad (\text{S108})$$

For a finite linewidth of the mode, the resulting $P(E)$ -function broadens accordingly,

$$P(E \approx n\hbar\omega_b) \approx e^{-\rho_b} \frac{\rho_b^n}{n!} \frac{2}{\pi} \frac{n\hbar\gamma_b}{(n\hbar\gamma_b)^2 + 4(E - n\hbar\omega_b)^2}. \quad (\text{S109})$$

Similarly, we will superpose this (real part of the) impedance by another Lorentzian peak, this time at frequency ω_a , describing resonator a .

Using above formulas, we can derive first a rough estimate for the photon flux density in the absence of input radiation, which implies its tendency as a function of resonator parameters. An accurate estimate for the photon flux density has to be done by evaluating the photon flux density numerically.

The first observation we make is that the emission rate is proportional to E_J^2 , which implies that we should minimize E_J to minimize spurious emission. This occurs when $g_a = 1$ and $g_b = \sqrt{n}$ (keeping $\epsilon_n = 1$). This is probably close to the most optimal situation when all terms beyond the rotating-wave approximation are accounted for. However, when studying barely the spontaneous emission rates, from Eq. (S109) we learn that $P(E)$ is actually proportional to $e^{-\rho_a - \rho_b}$, which cancels the same term appearing in the formula for E_J^* . Furthermore, if we assume that the leakage process involves emission of one photon to resonator b and one photon to frequency $\omega_J - \omega_b$, we get an additional proportionality to ρ_b . This implies for the total photon flux at frequency ω_b (within certain bandwidth) behaves as

$$f_{\omega_b} \equiv \int_{\omega_b} d\omega f(\omega) \propto n \times n! \frac{1}{g_a^2 g_b^{2(n-1)}}. \quad (\text{S110})$$

Assuming that at frequency $\omega_J - \omega_b$ the impedance contributes with a real number Z , and using the approximation $P(E) = e^{-\rho_a - \rho_b} 2\rho/\hbar(\omega_J - \omega_b)$ in this region, where $\rho = Z/R_Q$, we obtain the photon flux

$$f_{\omega_b} = \pi \frac{\gamma_a \gamma_b}{\omega_J - \omega_b} \frac{n \times n!}{g_a^2 g_b^{2(n-1)}} \frac{Z}{R_Q}. \quad (\text{S111})$$

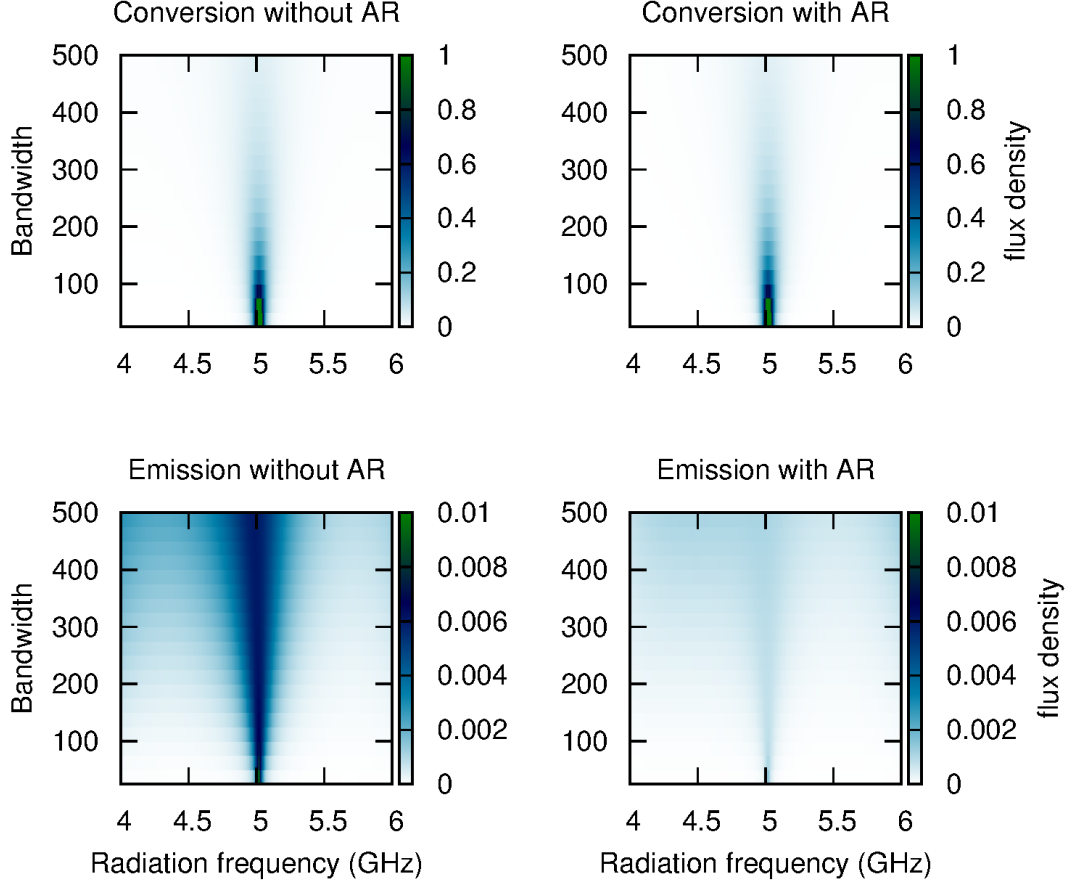


FIG. S4: Perturbative results for the emission photon flux density (in a.u.) in the presence of incoming radiation [top, Eq. (S105)] using $m = 1$, $J_1 = 1$, $J_{m \neq 1} = 0$], and emission photon flux density in the absence of input radiation [bottom, Eq. (S101)], with (right) and without (left) an anti-resonance (AR). We use the same normalization in all the plots. We consider the case of producing 3×5 GHz photons from a single 6.4 GHz photon with $2eV/h = 8.6$ GHz, and an AR at $\delta\omega/2\pi = 8.6 - 5 = 3.6$ GHz. The presence of the AR does not affect to conversion, but reduces the emission without input roughly by an order of magnitude. The total photon flux, presented in the main part of the article, is the integrated flux density between 4.5 – 5.5 GHz. We assume a temperature 20 mK and add the resonator impedances to Ohmic resistance $Z_0 = 50 \Omega$ with cut-off defined by $C = 0.1$ pF.

Eq. (S111) is an estimate how the decay rate behaves as a function of couplings g and decays γ . The impedance Z at frequency $\omega_J - \omega_b$ depends on the realization. The equation implies that having $Z = 0$, the rate vanishes completely. This is not true, because the energy $\hbar\omega_J - \hbar\omega_b$ can also be dissipated in the form of two photons at other frequencies. We, therefore, have to rely on numerical simulations.

To analyze the effect of anti-resonances, which can be used to reduce emission without input, we modify the impedance $\text{Re}[Z_t(\omega)]$ to

$$\text{Re}[Z_t(\omega)] \rightarrow \text{Re}[Z_t(\omega)] \times \left[1 - e^{(\omega - \omega_{\text{ar}})^2 / 2\Delta^2}\right]. \quad (\text{S112})$$

In the numerical simulations we use width $\Delta/2\pi = 0.5$ GHz. In the case of producing 3×6.4 GHz photons from a single 11.5 GHz photon we have $2eV/h = 7.7$ GHz and we use an anti-resonance at $\omega_{\text{ar}}/2\pi = 7.7 - 6.4 = 1.3$ GHz. In the case of producing 3×5 GHz photons from a single 6.4 GHz photon we have $2eV/h = 8.6$ GHz and we use an anti-resonance at $\omega_{\text{ar}}/2\pi = 8.6 - 5 = 3.6$ GHz. In the case of producing 2×11.5 GHz photons from a single 5 GHz photon we have $2eV/h = 18$ GHz. Here we need to use two anti-resonances, the first one at $\omega_{\text{ar}}/2\pi = 18 - 11.5 = 6.5$ GHz and the second one at $\omega_{\text{ar}}/2\pi = 18 - 11.5 - 5 = 1.5$ GHz.

At the same time, we verify that the perturbative result for the conversion rate is not changed due to anti-resonances in the environmental impedance. An example of the obtained photon flux densities is shown in Fig. S4.